



HAL
open science

Modeling plutonium sorption to kaolinite: Accounting for redox equilibria and the stability of surface species

Remi Marsac, Nidhu L Banik, Johannes Lützenkirchen, Razvan A Buda, Jens Kratz, Christian M. Marquardt

► To cite this version:

Remi Marsac, Nidhu L Banik, Johannes Lützenkirchen, Razvan A Buda, Jens Kratz, et al.. Modeling plutonium sorption to kaolinite: Accounting for redox equilibria and the stability of surface species. *Chemical Geology*, 2015, 400, pp.1 - 10. 10.1016/j.chemgeo.2015.02.006 . hal-01904144

HAL Id: hal-01904144

<https://hal.science/hal-01904144>

Submitted on 24 Oct 2018

HAL is a multi-disciplinary open access archive for the deposit and dissemination of scientific research documents, whether they are published or not. The documents may come from teaching and research institutions in France or abroad, or from public or private research centers.

L'archive ouverte pluridisciplinaire **HAL**, est destinée au dépôt et à la diffusion de documents scientifiques de niveau recherche, publiés ou non, émanant des établissements d'enseignement et de recherche français ou étrangers, des laboratoires publics ou privés.

1 **Modeling plutonium sorption to kaolinite:**
2 **accounting for redox equilibria and the**
3 **stability of surface species**
4

5 Rémi Marsac¹, Nidhu L. Banik^{1,*}, Johannes Lützenkirchen¹, Razvan A. Buda², Jens V.

6 Kratz², Christian M. Marquardt¹
7
8
9
10

11 ¹ Institut für Nukleare Entsorgung, Karlsruhe Institute of Technology, P.O. Box 3640, D-76021
12 Karlsruhe, Germany.

13 ² Institute for Nuclear Chemistry, University of Mainz, 55099 Mainz, Germany

14 *Corresponding author: E-mail address: nidhu.banik@kit.edu.

15 Tel +4972160822420; Fax: +4972160823927
16

17 **Abstract.** Plutonium with its particularly complex redox chemistry may be
18 thermodynamically stable in the states +III to +VI depending on the redox conditions in the
19 environment. Mineral surfaces can also affect Pu redox speciation. Therefore, the
20 interpretation of Pu sorption data becomes particularly challenging, even for simplified
21 laboratory experiments. The present study focuses on Pu sorption to kaolinite. Am(III),
22 Th(IV), Np(V) and U(VI) literature sorption data are used as analogues for the corresponding
23 Pu redox states to calibrate a simple surface complexation model, and the Nernst formalism is
24 applied. Two independent pH-pe diagrams, one for the kaolinite surface and another for the
25 aqueous phase, are constructed and superimposed. This allows visualization of the prevalent
26 Pu redox state in both phases. The model suggests that the stability field of the most strongly
27 adsorbing redox state is larger at the surface than in solution. Because Pu(V) weakly sorbs to
28 kaolinite, it never prevails at the surface. Within the stability field of Pu(V) in 0.1M NaClO₄
29 solution, Pu(VI) and Pu(IV) prevail at the kaolinite surface under oxidizing and slightly
30 reducing conditions, respectively. By contrast, the Pu(IV)/Pu(III) boundary is hardly affected
31 because both redox states strongly sorb to kaolinite, especially for pH > 6. The present
32 method is applied to literature data for Pu sorption to kaolinite. By estimating the pe from a
33 Pu redox state analysis in solution, overall Pu uptake could be predicted. Generic equations
34 are derived that are applicable to minerals and actinides other than kaolinite and Pu. The
35 present study provides important progress in understanding Pu geochemistry, especially in the
36 context of nuclear waste disposal where thermodynamic models are particularly necessary to
37 predict Pu mobility.

38 **Keywords:** Plutonium, kaolinite, redox, surface complexation modeling.

39 **Highlights:**

- 40 • Data of actinide analogues are used to model Pu(III,IV,V,VI) sorption to kaolinite.
- 41 • Two pH-pe diagrams for Pu are drawn for (i) the solution and (ii) the surface.
- 42 • Pu sorption and redox speciation can be predicted.
- 43 • The redox potential is crucial information: it controls Pu overall sorption.
- 44 • This approach can be applied to other minerals and actinides.

45

46

1. Introduction

47 Due to its radiotoxicity and the very long half-lives of several isotopes, plutonium (Pu)
48 is an important element in the context of nuclear waste disposal as well as in remediation of
49 areas contaminated by nuclear weapon testing or nuclear power-plant accidents. Geochemical
50 behavior of Pu is particularly challenging since, in environmentally relevant conditions, Pu
51 can be found in the oxidation states +III, +IV, +V or +VI. Pu(III) or Pu(IV) prevail under
52 reducing conditions, which are particularly relevant for deep geological nuclear waste
53 disposal. Pu(V) or Pu(VI) are more relevant under oxidizing conditions like oxygenated
54 surface environments. The chemical behavior of Pu concerning complexation by organic and
55 inorganic ligands, solubility, as well as sorption to minerals, strongly depends on the Pu redox
56 state (e.g. Altmaier et al., 2013). Thus, Pu(V) weakly sorbs to minerals and is considered to be
57 rather mobile (e.g. Geckeis et al., 2013). Pu(VI) and Pu(III) sorption is pH dependent and can
58 be affected by the presence of carbonates (especially for Pu(VI)). Pu(IV) strongly sorbs to
59 minerals, is sparingly soluble and, therefore, considered to be rather immobile. However,
60 Pu(IV) also tends to form intrinsic colloids in neutral to alkaline conditions, which might
61 enhance its mobility (Neck et al., 2007; Kersting, 2013; Walther and Denecke, 2013).
62 Consequently, sound knowledge of the geochemical behavior of each Pu redox state is
63 required to understand and predict Pu mobility in the environment. In this context, the
64 development of geochemical models that predict Pu speciation accounting for all these
65 processes are required.

66 Sorption to mineral surfaces can retard Pu migration or mediate its migration when Pu
67 sorbs to mineral colloids (Kersting et al., 1999; Xie et al., 2013), if these colloids remain
68 stable in aqueous suspension and can be transported by water flow. Because of the complexity
69 of the mineral-water interface and of the heterogeneity of minerals in nature, laboratory
70 studies with purified or synthetic minerals are carried out to unravel the underlying processes.

71 Even though such simplified systems have been widely investigated, the chemical behavior of
72 Pu still remains unclear. In particular, although introduced in a single redox state to a mineral
73 suspension, a mixture of Pu redox states rapidly emerges. For instance, when added either as
74 Pu(VI) or Pu(V) under ambient (air) atmosphere, Pu(V) prevails in solution at the end of the
75 experiment, but Pu(IV) is found at the surface of hematite, goethite, magnetite (Powell et al.,
76 2004; 2005; Romanchuk et al., 2011; 2013; Hixon and Powell, 2014), quartz/silica (Kumar et
77 al., 2012; Hixon et al., 2013) or montmorillonite (Zavarin et al., 2012). Similar observations
78 were recently made in the case of neptunium (Np) interaction with illite (Marsac et al., 2015).
79 Although initially introduced as Np(V) under oxygen-free argon atmosphere, a significant
80 amount of Np(IV) was found at the surface, whereas a small fraction remained in solution as
81 Np(V). Conversely, when Pu(IV) was added either under argon or ambient atmosphere, Pu(V)
82 was found in solution in the presence of kaolinite (Banik et al., 2007). Pu(III) sorption to
83 minerals has been probed less frequently, although it has high environmental relevance
84 (Kaplan et al., 2007; Lujanienė et al., 2009; Kirsch et al., 2011). Buda et al. (2008) reacted
85 Pu(III) with kaolinite in the presence of $\text{NH}_2\text{OH}\cdot\text{HCl}$ as reducing agent. A preliminary
86 experiment, in the absence of kaolinite, showed that Pu(III) was not stable and Pu(IV) formed
87 in solution in the presence of $\text{NH}_2\text{OH}\cdot\text{HCl}$ for $\text{pH} > 6$. In the presence of kaolinite, the pH-
88 edges of Pu and Am(III) were found to be very similar, the sorption plateau being reached for
89 $\text{pH} \approx 6$. This suggests that the Pu(IV)/Pu(III) redox couple is only weakly affected by sorption.

90 It appears from all these studies that mineral surfaces have a strong impact on Pu
91 redox speciation, especially when the Pu(V)/Pu(IV) couple is involved. Furthermore, these
92 studies also show that the prevalent redox state of the metal ion in aqueous solution can differ
93 from that at the mineral surface. In principle, the overall redox potential of the system should
94 determine the final redox state of Pu (Geckeis et al., 2013). It has been previously proposed
95 that the strongly adsorbing Pu(IV) is thermodynamically favored at a mineral surface

96 compared to Pu(V) (Hixon et al., 2013; Hixon and Powell, 2014). With such an approach, the
97 Np sorption to illite and redox speciation could recently be described in a quantitative way
98 considering Np(IV) at the mineral surface and Np(V) in solution (Marsac et al., 2015). This
99 approach might also be suitable in the case of Pu, because of the very similar chemistry of
100 both actinides.

101 To determine the stability fields of different Pu redox states at a mineral surface, the
102 sorption behavior of all redox states must be known separately. It appears that for Pu such
103 experimental data will hardly ever become available because a mixture of redox states is
104 found in most experimental studies. Fortunately, lanthanides/actinides (Ln/An) exhibit similar
105 chemical behavior for the same redox state, even though thermodynamic constants may
106 significantly differ between two elements (Altmaier et al., 2013). The use of these elements as
107 chemical analogues might help to unravel the complex geochemical behavior of Pu in a first
108 approach (Choppin, 1999).

109 The present study focuses on kaolinite because experimental sorption data for
110 americium(III) (Am^{3+}), thorium(IV) (Th^{4+}), neptunium(V) (NpO_2^+) and uranium(VI) (UO_2^{2+})
111 are available (Buda et al., 2008; Banik et al., 2007; Amayri et al., 2011; Křepelová, 2007).
112 These data are assumed to be representative for sorption of Pu(III, IV, V, VI), respectively,
113 and used for each redox state of Pu to calibrate the simple surface complexation model
114 developed by Tertre et al. (2008). By merging Pu redox chemistry with sorption processes, the
115 resulting model is used to construct a predominance (pH-pe) diagram for Pu redox speciation
116 at the kaolinite surface. The modeling results are compared with experimental data in order to
117 test the capacity of the model to predict Pu sorption to kaolinite as a function of pH and pe.
118 The present approach is subsequently tested on metal sorption on other minerals.

119

120

2. Materials and method

121 2.1. Geochemical speciation code and thermodynamic database

122 PHREEQC (version 2; Parkhurst and Appelo, 1999) is a computer code that can
123 perform speciation (including surface complexation) and saturation-index calculations in
124 water. Predominance (pH-pe) diagrams can be obtained using PhreePlot (Kinniburgh and
125 Cooper, 2009), which contains an embedded version of PHREEQC. In the present work,
126 thermodynamic constants for Pu aqueous speciation and solubility are taken from the NEA
127 thermodynamic database (Guillaumont et al., 2003). Reactions and corresponding
128 thermodynamic constants at 25°C and zero ionic strength are given in Table 1. In case of gaps
129 in the Pu database, data for analogues were chosen and are included in Table 1. A redox
130 reaction involving aqueous Pu^{4+} and PuO_2^+ is not given. It is calculated based on the reaction
131 $\text{PuO}_{2(\text{am,hyd})} = \text{PuO}_2^+ + \text{e}^-$ with $\log K = -19.78$ at zero ionic strength (Guillaumont et al., 2003).
132 The specific ion interaction theory (SIT; Ciavatta, 1980) accounts for ionic strength effects
133 and the corresponding parameters for Pu (or the chosen analogue) from Guillaumont et al.
134 (2003) are used.

135

136 2.2. Surface complexation modeling

137 As for other clay minerals, the kaolinite surface is complex because of the presence of
138 various types of hydroxyl surface groups, mainly silanols ($\equiv\text{SiOH}$) and aluminols ($\equiv\text{AlOH}$),
139 that can bind cations. Furthermore, several faces with different charging properties occur
140 (Miller et al., 2007) making the development of mechanistic models a challenging task. Tertre
141 et al. (2008) showed that batch uptake data for the trivalent lanthanides to kaolinite can be
142 relatively well modelled by the “Generalized Composite Approach” (Davis et al., 1998;
143 Davies et al., 2004). In this approach, only one type of generic surface site ($\equiv\text{SOH}$) is

144 considered and no electrostatic term is included. As detailed by Tertre et al. (2008), for the
 145 modeling of the actinide sorption to kaolinite acid-base properties of the surface do not need
 146 to be treated explicitly. A similar approach was also used by Lützenkirchen (2012). The
 147 general reaction equation for the complexation of an actinide (An) cation with a charge “+n”
 148 to a monodentate generic surface group ($\equiv\text{SOH}$) can be written tentatively as:



150 where $i \geq 1$. The corresponding surface complexation constant will be noted ${}^{\text{S}}\text{K}_{\text{X},(i-1)}$, where
 151 “X” denotes the redox state of the actinide. In the case of lanthanides (e.g. europium; Eu),
 152 Tertre et al. (2008) only consider the formation of the surface species $\equiv\text{SOEu}^{2+}$. Their study
 153 was restricted to $\text{pH} < 8$ and a decrease in the simulated sorption between $\text{pH} 7$ and 8 suggests
 154 that more (hydrolyzed) surface species (e.g. $\equiv\text{SOEuOH}^+$) need to be considered for $\text{pH} > 8$.
 155 This is similar to other clay minerals whenever a non-electrostatic model is used (e.g. for
 156 montmorillonite or illite: Bradbury and Baeyens 2005; 2009). In addition, cation exchange is
 157 a relevant sorption mechanism in the case of kaolinite. In PHREEQC, the Gaines and Thomas
 158 (1953) convention can be used, whereby cation exchange reactions, the thermodynamic
 159 exchange constant (K_{exch}), and selectivity coefficient (${}^{\text{An}}\text{K}_{\text{C}}$) are expressed as follows:



$$161 \quad K_{\text{ex}} = \frac{N_{\text{An}}}{(N_{\text{Na}})^n} \times \frac{f_{\text{An}} [\text{Na}^+]^n}{(f_{\text{Na}})^n [\text{An}^{n+}]} = \frac{{}^{\text{An}}\text{K}_{\text{C}}}{(f_{\text{Na}})^n} \quad (3)$$

162 Here, N_i are equivalent fractions, f_i are surface activity coefficients and brackets denote
 163 activities in solution. Tertre et al. (2008) also considered a H^+ - Na^+ exchange reaction with log

$$164 \quad {}^{\text{H}}\text{K}_{\text{C}} = -1.$$

165 In the case of the original study of Tertre et al. (2006, 2008), the surface area of
166 kaolinite is 10 m²/g, site densities for ≡SOH and exchange sites are 1.66 and 3.70 μmol/m²,
167 respectively.

168

169 **2.3. Distribution coefficients (K_d)**

170 As will be shown in the next sections, the use of distribution coefficients (K_d) to
171 express An uptake by kaolinite is particularly convenient for the present purpose. K_d is
172 defined as:

$$173 \quad K_d = \frac{[An]_{surf}}{[An]_{tot,aq}} \times \frac{V}{S} \quad (4)$$

174 where [An]_{surf} and [An]_{tot,aq} refer to the total amount (i.e. the sum of all the species including
175 various redox states) at the surface and in solution, respectively, and V/S is the liquid to solid
176 ratio. S can be either expressed as the mass of solid (K_d in L/kg) or as the surface area (K_d in
177 L/m²) in contact with a given solution volume. K_d is a highly conditional parameter that
178 depends on the physico-chemical conditions (e.g. pH, I, T, ligands in solution, surface
179 loading). As discussed later, this study focused on data obtained at room temperature, for 0.1
180 M NaClO₄, in the absence of complexing ligands other than OH⁻ and assuming ideal sorption
181 behavior. Therefore, the evolution of K_d with pH can be calculated using the simple surface
182 complexation model described above.

183 K_d is commonly experimentally determined to quantify actinide sorption to minerals.
184 In the case of redox sensitive elements like Pu, several redox states (Pu(X); X = III, IV, V, or
185 VI) might occur simultaneously both at the surface and in the aqueous phase, depending on
186 the redox conditions. The overall (measured) K_d will be ultimately affected by the Pu redox
187 state distribution. For a mixture, K_d is denoted K_{d,tot} and can be written as follows:

188
$$K_{d,tot} = \frac{\sum_X [Pu(X)]_{surf}}{\sum_X [Pu(X)]_{tot,aq}} \times \frac{V}{S} = \frac{\sum_X K_d(X) \times [Pu(X)]_{tot,aq}}{\sum_X [Pu(X)]_{tot,aq}} \quad (5)$$

189 $K_d(X)$ represents the measured K_d for the ideal case where only the redox state X is present
 190 both at the surface and in solution (i.e. when $K_{d,tot} = K_d(X)$):

191
$$K_d(X) = \frac{[Pu(X)]_{surf}}{[Pu(X)]_{tot,aq}} \times \frac{V}{S} \quad (6)$$

192 Such values can conveniently be obtained for redox insensitive analogues and applied to Pu.

193

194 **2.4. Predominance pH-pe diagram**

195 *2.4.1. Construction of a simplified predominance diagram for aqueous species*

196 For simplicity, in the remainder of the text, we used brackets to denote concentrations
 197 and K will refer to the conditional constant valid for a given ionic strength. In practice,
 198 appropriate corrections of the stability constants for $I = 0$ can be handled by speciation codes
 199 like PHREEQC applying appropriate activity corrections for example by using SIT. This
 200 study will only focus on experimental data obtained in non-complexing background
 201 electrolyte solutions ($NaClO_4$), under inert atmosphere or under atmospheric conditions where
 202 carbonate complexation was shown to be negligible (i.e. for sufficiently low pH). Furthermore,
 203 we restrict the study to sufficiently low Pu concentrations such that the formation of dissolved
 204 polycations is negligible. Under these premises, only the hydrolysis of Pu(III, IV, V, VI) are
 205 taken into account in the following equations. They are not valid in the presence of other
 206 complexing ligands (e.g. carbonates), but can be extended to include effects of aqueous
 207 speciation beyond bare hydrolysis in the absence of ternary surface complexes.

208 Free aqueous component species of Pu are Pu^{3+} , Pu^{4+} , PuO_2^+ and PuO_2^{2+} for the
 209 successive redox states. All relevant reactions are given in table 1. A generic redox reaction of
 210 an oxidized (Pu(Ox)) to a reduced (Pu(Red)) form can be written as:



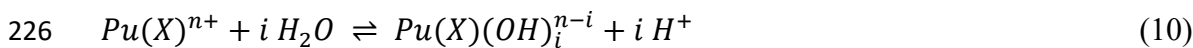
$$212 \quad K_{\text{Ox/Red}} = \frac{[\text{Pu}(\text{Red})^{(n-q+m)}]}{[\text{Pu}(\text{Ox})^{n+}][\text{H}^+]^m[\text{e}^-]^q} \quad (8)$$

213 The simplified reaction 7, where “n” is the charge of the free Pu(Ox) cation, “q” is the number of
 214 electrons involved and “m” equals 0 or 4 depending on the redox states involved, is not
 215 entirely balanced because the “plutonyl oxygens” are not shown (see table 1). As an example,
 216 the reduction reaction of PuO_2^{2+} to Pu^{4+} involves two electrons and four protons ($q = 2$; $m = 4$)
 217 whereas Pu^{4+} reduction to Pu^{3+} involves only one electron ($q = 1$; $m = 0$). The mass law
 218 equation can be rearranged as follows:

$$219 \quad pe = \log K_{\text{Ox/Red}}/q + \log \left(\frac{[\text{Pu}(\text{Ox})^{n+}]}{[\text{Pu}(\text{Red})^{(n-q+m)}]} \right) /q - m/q \times pH \quad (9)$$

220 where pe equals $-\log a_e$ (the apparent activity of the electron). pe is related to the redox
 221 potential (in Volts, versus the standard hydrogen electrode) by the relationship: $pe = 16.9 \times E_h$,
 222 at 25°C. Applying the latter convention to eq. 9 would lead to the well-known Nernst
 223 equation. For standard conditions (25°C, pH = 0 and zero ionic strength) when $[\text{Pu}(\text{Ox})^{n+}] =$
 224 $[\text{Pu}(\text{Red})^{(n-q+m)}]$, the standard redox potential E^0 for a given couple is obtained.

225 The general hydrolysis reaction of a given Pu redox state “X” is:



$$227 \quad {}^{OH}K_{X,i} = \frac{[\text{Pu}(\text{X})(\text{OH})_i^{n-i}][\text{H}^+]^i}{[\text{Pu}(\text{X})^{n+}]} \quad (11)$$

228 where $^{OH}K_{X,i}$ is the corresponding equilibrium constant. The total aqueous concentration of
 229 Pu(X) ($[Pu(X)]_{tot, aq}$) can be calculated from the concentration of the free cation ($[Pu(X)^{n+}]$) via:

$$230 \quad [Pu(X)]_{tot, aq} = [Pu(X)^{n+}] + \sum_i [Pu(X)(OH)_i^{n-i}] = [Pu(X)^{n+}] \times \left(1 + \sum_i \frac{^{OH}K_{X,i}}{[H^+]^i} \right)$$

$$231 \quad = [Pu(X)^{n+}] \times \alpha_X \quad (12)$$

232 where α_X is the side reaction coefficient for Pu(X). Introduction in the Nernst equation (eq. 9)
 233 yields:

$$234 \quad pe = \log K_{Ox/Red} / q + \log \left(\frac{[Pu(Ox)]_{tot, aq}}{[Pu(Red)]_{tot, aq}} \times \frac{\alpha_{Red}}{\alpha_{Ox}} \right) / q - m/q \times pH \quad (13)$$

235 The pe corresponding to the borderline between two Pu redox states in solution (noted
 236 $\{Ox/Red\}_{aq}$) is found as follows:

$$237 \quad \{Ox/Red\}_{aq} = pe = \log K_{Ox/Red} / q + \log \left(\frac{\alpha_{Red}}{\alpha_{Ox}} \right) / q - m/q \times pH \quad (14)$$

238 $\{Ox/Red\}_{aq}$ evolves with pH and ionic strength. With eq. 14, a relatively simple
 239 predominance (pH-pe) diagram can be drawn. It will not show the speciation of a given redox
 240 state (e.g. hydrolyzed species) but the boundaries between redox states appear. In eq. 14, the
 241 side reaction coefficient ratio is driving $\{Ox/Red\}_{aq}$, i.e. the redox state of Pu with the
 242 strongest hydrolysis tends to enlarge its predominance area with increasing pH. Note that the
 243 precipitation of solid phases is not included in the present calculations. Therefore, the
 244 equations are only valid (i) below the saturation of relevant Pu-bearing minerals or (ii) for
 245 discussions restricted to the aqueous phase, independent of any solid phase (i.e. precipitates as
 246 well as adsorbing phase), as discussed by Schüring et al. (2000).

247

248

249 **2.4.2. Construction of a predominance diagram for the mineral surface**

250 To take into account sorption processes in the Nernst equation, the expression of K_d
251 (eq. 6) for two different redox states (i.e. $K_d(Ox)$ and $K_d(Red)$) can be included into eq. 13:

252
$$pe = \log K_{Ox/Red} / q + \log \left(\frac{[Pu(Ox)]_{surf}}{[Pu(Red)]_{surf}} \times \frac{\alpha_{Red}}{\alpha_{Ox}} \times \frac{K_d(Red)}{K_d(Ox)} \right) / q - m/q \times pH \quad (15)$$

253 and it becomes possible to calculate the predominance field for different Pu surface redox
254 states. Because eq. 15 exclusively relates to the surface, such a plot is independent of that
255 corresponding to solution: both must be superimposed for comparison. As stated before, K_d
256 varies with pH and ionic strength.

257 On a pH-pe diagram, the borderline between two redox states at the mineral surface
258 ($\{Ox/Red\}_{surf}$) can be directly compared with the one in solution:

259
$$\{Ox/Red\}_{surf} = \{Ox/Red\}_{aq} + (\log K_d(Red) - \log K_d(Ox))/q \quad (16)$$

260 At the mineral surface, the pH-pe predominance area of the redox state with the strongest
261 sorption behavior (i.e. the highest K_d) is enlarged relative to the aqueous phase, similar to the
262 effect of hydrolysis in solution. Hence, certain redox conditions will favor the stabilization of
263 a given redox state in solution whereas the corresponding reduced or oxidized form is
264 stabilized at the surface. The pe scale appears more appropriate than Eh since, for a reaction
265 involving only one electron ($q = 1$), a difference of one order of magnitude between the K_d 's
266 ($\Delta \log K_d = 1$) simply shifts the Ox:Red 1:1 borderline at the mineral surface compared to the
267 one in solution by one pe unit (± 60 mV). Such uncertainties on pe are on the order of
268 experimental errors (Altmaier et al., 2010).

269

270

271 2.5. Data selection

272 Because of its complex redox chemistry, the ideal pH-edges of Pu(III/IV/V/VI) for
273 one redox state in the system are not readily available. Fortunately, f-orbital elements exhibit
274 very similar chemical behaviors for a given redox state, and the nearest neighbors in the
275 lanthanide and actinide series of the periodic table show sufficiently similar chemistries to
276 serve as analogues. In this study, experimental uptake data on kaolinite for Am(III), Th(IV),
277 Np(V) and U(VI) are assumed to be representative for the sorption of Pu in the corresponding
278 redox state. These experimental data can then be directly used to calibrate the surface
279 complexation model Pu(III/IV/V/VI). The subsequent predictions of this model will strongly
280 depend on this approximation.

281 Experimental datasets for Am(III) (Buda et al., 2008; $[Am]_{tot} = 10^{-9}$ M), Th(IV) (Banik
282 et al., 2007; $[Th]_{tot} = 6.6 \times 10^{-13}$ M) and Np(V) (Amayri et al., 2011, $[Np]_{tot} = 7 \times 10^{-12}$ M) are
283 chosen. All these studies on actinide sorption involve kaolinite KGa-1b at 4 g/L, 0.1 M
284 NaClO₄ background electrolyte and absence of CO₂. The above elements are very stable in
285 the respective redox states for a wide range of pH-pe conditions. However, under inert
286 atmosphere (i.e. Ar), Np(V) was partially reduced to Np(IV) in the presence of illite, leading
287 to higher overall uptake compared to Np(V) sorption to illite in the presence of O₂ (Gorgeon,
288 1994; Marsac et al., 2015). Nevertheless, for pH < 7, where carbonates have no influence on
289 Np(V) sorption to kaolinite, Amayri et al. (2011) found similar results under inert and
290 ambient atmospheres. Therefore, their Np-kaolinite data can be confidently attributed to the
291 sorption of Np(V) only. By contrast, U(VI) sorption to kaolinite, often studied in the presence
292 of CO₂ (e.g. Payne et al., 2004; Gao et al., 2010), is strongly affected by U(VI)-carbonate
293 complexation for pH > 8. Fortunately, Křepelová (2007) investigated U(VI) sorption to KGa-
294 1b in 0.1 M NaClO₄ with CO₂ and in 0.01 M NaClO₄ in the absence of CO₂ ($[U]_{tot} = 10^{-6}$ M;

295 S/V = 4 g/L). Both data sets will be discussed, discarding the sorption data above pH = 8 in
296 the presence of CO₂. The published data were digitized and recalculated to K_d (eq. 4).

297 The sorption of Am(III), Th(IV), Np(V) and U(VI) to kaolinite has been studied for
298 different [An]_{tot} (from 6.6×10⁻¹³ to 10⁻⁶ M). Uptake of An on kaolinite may in principle be
299 affected by the total An concentration due to the presence of low and high affinity sites in
300 different amounts, causing non-ideal sorption behavior at the respective An to kaolinite ratios.
301 A lower uptake was measured for Np(V) and U(VI) in the corresponding studies for higher
302 [Np/U]_{tot} (~10⁻⁵ M), which can be attributed to a surface site saturation effect. The behavior of
303 An at such high concentrations is not addressed in this study. The modeling of An uptake by
304 kaolinite is restricted to the lowest [An]_{tot} available in the literature. Although ideal sorption
305 behavior was established for low [An]_{tot} in the case of illite and montmorillonite (Bradbury
306 and Baeyens, 2005; 2009), this observation cannot a priori be transferred to kaolinite due to
307 the lack of sorption isotherms for each of the analogues of Pu(III, IV, V, VI) over sufficiently
308 broad [An]_{tot} ranges (especially for very low [An]_{tot}). As a first approximation our treatment
309 assumes ideal sorption behavior for all An. If the simulations result in reasonable prediction
310 of the experimental data, this simplification is appropriate for the range of conditions of the
311 calibration and simulation data sets. Any prediction made with this model for environmentally
312 relevant Pu concentrations (e.g. ~10⁴ atoms/kg in Dai et al., 2002) should be considered with
313 caution.

314 Banik et al. (2007) added Pu(IV) ($6.9 \times 10^{-9} < [\text{Pu}]_{\text{tot}} < 3.5 \times 10^{-7}$ M) to a KGa-1b
315 suspension (S/V = 4 g/L) in 0.1 M NaClO₄ either under argon or ambient atmosphere.
316 Detailed information on the experimental work can be found in Banik (2006). In that study,
317 only small variations in Pu uptake were observed (i) with time between 63 and 209 h (Figure
318 S1), (ii) with [Pu]_{tot} (Figure S2) and (iii) with changes of the atmosphere for pH < 9. However,
319 speciation calculations suggested that significant amounts of Pu-carbonate complexes formed

320 for $\text{pH} > 8$ in the presence of CO_2 . We will not discuss the effect of carbonate in the present
321 study so the latter data for $\text{pH} > 8$ in the presence of CO_2 are not considered. Pu aqueous
322 redox state analysis ($\pm 10\%$ uncertainty) in the solution on contact with kaolinite and
323 subsequent phase separation (i.e. only the aqueous phase was analyzed) was performed at pH
324 = 1, 4 and 9 ($[\text{Pu}]_{\text{tot}} = 3.5 \times 10^{-7} \text{ M}$), resulting in (i) for $\text{pH} = 1$, 38% of Pu(III) and 46% of
325 Pu(IV), (ii) for $\text{pH} = 4$, 75% of Pu(V) and 14% of Pu(IV) and (iii) for $\text{pH} = 9$, 45% of Pu(IV)
326 and 49% of Pu(IV) in form of intrinsic (or eigen-) colloids.

327

328

3. Results and discussion

3.1. Surface complexation modeling

330 Figure 1 presents the experimental $\log K_d$ values (in L/kg) versus pH for Am(III),
331 Th(IV) and Np(V) sorption to kaolinite ($S/V = 4 \text{ g/L}$) in 0.1 M NaClO_4 and in the absence of
332 CO_2 from the literature (Buda et al., 2008; Banik et al., 2007; Amayri et al., 2011). Both the
333 U(VI) sorption data of Křepelová (2007) in 0.1 M NaClO_4 with CO_2 ($\text{pH} < 8$) and in 0.01 M
334 NaClO_4 without CO_2 are shown. When plotted as $\log K_d$, the two latter datasets are similar,
335 showing that U(VI) sorption to kaolinite is barely affected by ionic strength. Only a slightly
336 higher sorption is observed in 0.01 M NaClO_4 . The pH -edges follow the effective charge of
337 the cations $\text{Np(V)} (+2.3) < \text{Am(III)} (+3) < \text{U(VI)} (+3.3) < \text{Th(IV)} (+4)$, as usual (Geckeis et
338 al., 2013). Sorption reaches a plateau for all actinides at $3.5 < \log K_d < 4$, as well as for both
339 ionic strengths investigated for U(VI). K_d values cannot be derived for U(VI) ($\text{pH} < 4$) and
340 Np(V) ($\text{pH} < 6$) because no significant sorption occurred at the solid to liquid ratio of 4 g/L.
341 For $2 < \text{pH} < 4$, K_d for Am(III) remains constant, due to cation exchange, and lower sorption
342 is observed for $\text{pH} < 2$.

343 Am(III), Np(V), and U(VI) will provide a sound estimate for Pu(III/V/VI) sorption to
344 kaolinite due to the similar hydrolysis constants of the respective analogues. Direct
345 comparison between Th(IV) and Pu(IV) is hampered by the documented difference in their
346 hydrolysis constants. An inaccurate description of Pu(IV) sorption might have consequences
347 for the determination of the various boundaries between two Pu redox states on the kaolinite
348 surface ($\{Ox/Red\}_{surf}$). However, the difference between Th(IV) and Pu(IV) sorption must be
349 large (more than one log K_d unit) to significantly affect our interpretations, as discussed in
350 section 2.4.2. From the sorption data and the Pu redox state analysis in solution as reported by
351 Banik (2006), eq. 5 allows us to determine $K_d(IV)$, i.e. the K_d that is measured in the case
352 where only Pu(IV) would be present both at the surface and in solution. If Pu(IV) and an
353 additional redox state X prevail, eq. 5 becomes:

$$354 \quad K_d(IV) = (K_{d,tot} - K_d(X) \times F_{X,aq}) / F_{IV,aq} \quad (17)$$

355 where $F_{IV,aq}$ and $F_{X,aq}$ represent the fractions of the respective redox states in solution. With
356 equation 17, $K_d(IV)$ can be calculated for pH = 1, with $K_d(III)$ from Am(III). For pH = 4,
357 although 75% of Pu(V) was present in solution ($F_{V,aq} = 0.75$), Pu(V) sorption is weak and
358 $K_d(V) \times F_{V,aq}$ can be neglected. This leads to $K_d(IV) \approx K_{d,tot} / F_{IV,aq}$ (Figure 1). K_d values for
359 Th(IV) and Pu(IV) are very similar for kaolinite, which supports the use of Th(IV) as a
360 reliable analogue. For pH = 9, $K_d(IV)$ cannot be determined because Banik et al. (2007)
361 observed Pu(IV) as monomers or eigen-colloids. However, we expect a constant K_d for pH >
362 4 since tetravalent actinides show no hydrolyzed aqueous species beyond $An(OH)_{4(aq)}$ (e.g.
363 $An(OH)_5^-_{(aq)}$). Therefore, in the absence of CO_2 , no additional complexation reaction for
364 Pu(IV) in solution occurs that could decrease Pu sorption on kaolinite, relative to Th(IV), for
365 high pH.

366 The surface complexation constant for $\equiv\text{SOPu(III)}^{2+}$ is set equal to the one for Eu(III)
 367 ($\equiv\text{SOEu(III)}^{2+}$) determined by Tertre et al. (2008) (Table 1), since Eu(III) is as well an
 368 analogue for trivalent actinides. All the other surface complexation constants are fitted to the
 369 K_d of the respective analogues and are listed in table 1. A good fit is achieved with this simple
 370 model (Fig. 1). The fitted surface complexation constants ($\log {}^S K_{X,(i-1)}$; eq. 1) for
 371 Pu(III/IV/V/VI), when plotted against the corresponding hydrolysis constants ($\log {}^{OH} K_{X,i}$; eq.
 372 10), yield a linear free energy relationship (LFER; Figure 2):

$$373 \log {}^S K_{X,(i-1)} = 0.97 \times \log {}^{OH} K_{X,i} + 5.65 \quad (R^2 = 0.99) \quad (18)$$

374 The correlation corroborates the self-consistency of our surface complexation constants. The
 375 Na^+ - Pu^{3+} selectivity coefficient is found to be 10 ($\log {}^{Pu(III)}_{Na} K_c = 1$), in agreement with Tertre
 376 et al. (2008), and is relatively consistent with literature data of selectivity coefficients for
 377 An/Ln(III) with clay minerals (e.g. Bradbury and Baeyens, 2006; 2009) although it is found to
 378 be lower than for montmorillonite and illite ($\log {}^{Pu(III)}_{Na} K_c = 1.5$ and 1.9, respectively). The
 379 rather weak Am(III) uptake at pH = 1 is relatively well simulated when taking into account
 380 the Na^+ - H^+ exchange reaction previously considered by Tertre et al. (2008). During
 381 preliminary tests, when using the Na^+ - UO_2^{2+} selectivity coefficient reported for
 382 montmorillonite (Marques Fernandez et al., 2012), for 0.1 M NaClO_4 , the predicted $\log K_d(\text{VI})$
 383 for pH < 4 remained below the experimental data for pH = 4, while for 0.01 M NaClO_4 too
 384 high values were predicted. Since reliable exchange constants cannot be determined for U(VI)
 385 and Np(V) from the selected datasets, the ion exchange mechanism is omitted in the present
 386 study. However, this has no significant consequence for the following discussions and the
 387 approach can be extended to include ion exchange once reliable selectivity coefficients
 388 become available. Furthermore, Bradbury and Baeyens (2005) observed no effect of the ionic
 389 strength between 0.1 and 1 M (NaClO_4) for Th(IV) sorption to montmorillonite. Therefore,
 390 cation exchange for Pu(IV) is not considered. Kaolinite dissolution is not taken into account

391 in this study. Kaolinite dissolution could be affecting the amount of available surface sites or
392 result in competitive effects from dissolved aluminium (Lützenkirchen et al., 2014), for
393 instance. Finally, the present model is likely to be questionable for the very low pH values,
394 especially for $\text{pH} \approx 0$, but (i) such low pH values are of minor environmental relevance and (ii)
395 the equations derived in this study to describe Pu sorption and redox speciation at the
396 kaolinite surface are based on K_d values, and therefore this should have no impact on the
397 following discussions based on the results from laboratory experiments.

398

399 **3.2. Predominance diagram: solution versus surface**

400 Figure 3 shows the superimposed predominance diagrams for the different Pu redox
401 states in solution (in black) and at the kaolinite surface (in gray), in 0.1 M NaClO_4 and in the
402 absence of CO_2 . The ionic strength increases by a factor of about 10 between $\text{pH} = 1$ and 0
403 because of increasing $[\text{HClO}_4]$. Pu(IV) is found at intermediate redox conditions. Its
404 predominance area is small at low pH due to the similar standard redox potentials for the
405 different couples. When the pH increases, its stability field is enlarged because of its strong
406 hydrolysis. Pu(III) shows the largest stability field in acidic condition, which is narrowed with
407 increasing pH by hydrolyzed Pu(IV) species. Pu(VI) is only stable under oxidizing conditions.
408 Its stability field is increased for $\text{pH} > 8$ because of its relatively strong hydrolysis. Pu(V)
409 predominates in less oxidizing conditions than Pu(VI). Pu(V) shows very weak hydrolysis,
410 which explains its confined predominance field for alkaline pH.

411 From a purely thermodynamic point of view, if hydrolysis controls the predominance
412 area of the different redox states in solution, complexation reaction with the $-\text{OH}$ groups of
413 the kaolinite surface should act similarly (see Figure 3, in gray). For $\text{pH} < 6$, Pu(IV) sorption
414 to kaolinite is much stronger than Pu(III), narrowing the predominance area for surface Pu(III)

415 compared to solution. For $\text{pH} > 6$ both redox states exhibit similarly strong sorption, and
416 $\{\text{Pu(IV)/Pu(III)}\}_{\text{surf}}$ is close to $\{\text{Pu(IV)/Pu(III)}\}_{\text{aq}}$.

417 In the range of pH presently discussed, Pu(V) sorption is always weaker than for the
418 other redox states. Although present under some conditions, it never predominates and does
419 not appear in Figure 3. Instead Pu(IV) and Pu(VI) prevail at the kaolinite surface (depending
420 on the pe), even if Pu(V) is stable in solution.

421 $\{\text{Pu(VI)/Pu(IV)}\}_{\text{surf}}$ evolves in similar fashion as $\{\text{Pu(IV)/Pu(III)}\}_{\text{surf}}$: (i) the Pu(IV)
422 stability field at the kaolinite surface is enlarged because of the lower Pu(VI) sorption at low
423 pH , whereas for $\text{pH} > 6$ the Pu(VI)/Pu(IV) borderlines at the surface and in solution are
424 similar due to the similar K_d for both redox states. While significant Am(III) sorption to
425 kaolinite was experimentally observed in the pH range investigated, U(VI) sorption is
426 insignificant for $\text{pH} < 4$, leading to highly uncertain $K_d(\text{VI})$. Therefore, the calculated
427 $\{\text{Pu(VI)/Pu(IV)}\}_{\text{surf}}$ values for $\text{pH} < 4$ are probably inaccurate. Note also that
428 $\{\text{Pu(VI)/Pu(IV)}\}_{\text{surf}}$ is found for almost constant redox conditions: $\text{pH} + \text{pe} \approx 18$.

429 The present approach, which separates Pu redox speciation in solution and at the
430 surface, has the advantage of being insensitive to the solid to liquid ratio within a sufficiently
431 low $[\text{Pu(X)}]_{\text{tot}}$ range where K_d values remain constant (i.e. ideal sorption behavior). We may
432 simultaneously visualize the prevalent redox states in solution and at the surface. Such an
433 approach was also shown to be useful when mineral phases can form (Schüring et al., 2000).
434 It also turns out to be particularly useful to understand overall Pu uptake by kaolinite.
435 Common predominance diagrams would not separate Pu redox speciation in solution and at
436 the surface and only the prevalent species in the total system, either on the surface or in
437 solution, will appear. Such a diagram is shown in figure 3b for our experimental conditions
438 ($\text{S/V} = 4 \text{ g/L}$; 0.1 M NaClO_4). In our model, the comparison between Figure 3a and 3b shows
439 that although Pu(VI) is stable at the kaolinite surface under oxidizing conditions (Fig. 3a), it

440 represents only a small proportion of Pu because, below $\text{pH} < 7$, Pu(VI) sorption is weak and
441 Pu(V) prevails in solution (Fig. 3b). This strongly limits overall Pu sorption.

442

443 3.3. Pu(V) versus Pu(IV)

444 3.3.1. Modeling Pu-kaolinite sorption data

445 Our model is applied to the experimental data of Banik et al. (2007) where 6.6×10^{-9} M
446 of Pu(IV) was contacted with 4 g/L kaolinite in 0.1 M NaClO₄. The experimental percentage
447 of Pu uptake reported by Banik et al. (2007) in air (only for $\text{pH} < 8$) and in argon atmosphere
448 are shown in Figure 4a together with Th(IV) data ($[^{234}\text{Th}]_{\text{tot}} = 6.6 \times 10^{-13}$ M). Pu overall uptake
449 is systematically lower than Th(IV). Overall Pu uptake increases from 10 to 80% for $0 < \text{pH} <$
450 3 , decreases down to $\sim 60\%$ for pH around 4 and reaches again $\sim 80\%$ above $\text{pH} = 7$. The dip
451 at intermediate pH is unusual and cannot be explained by Pu(IV) alone, which becomes clear
452 from a redox state analysis of Pu in the aqueous phase.

453 No redox potential measurements were performed by Banik et al. (2007), which would
454 have been crucial information for the present study. Instead of using the measured p_e , we here
455 attempt to estimate the p_e via the Nernst equation and by using the Pu redox state analysis in
456 solution after reaction with kaolinite and subsequent phase separation. This approach has been
457 previously applied by Yun et al. (2007). However, those authors investigated acidic
458 conditions ($\text{pH} < 2.5$) and observed some discrepancies between calculated and measured p_e .
459 Therefore, we might obtain a p_e value with a relatively large uncertainty. In the modified
460 Nernst equation (eq. 13), the experimental total concentration of two Pu redox states and the
461 pH can be directly used to estimate the p_e . We obtain $p_e \approx 15.7$ for $\text{pH} = 1$ and $p_e \approx 11.6$ for
462 $\text{pH} = 4$, i.e. almost constant redox conditions (constant $\text{pH} + p_e \approx 16.1$). The redox state
463 analysis data cannot be used in eq. 13 for $\text{pH} = 9$ because only Pu(IV) was detected.

464 Additionally, the redox speciation has only been performed for the samples studied under
465 ambient conditions. Therefore, although a steady state was reached, as deduced from Pu
466 sorption behavior (Fig. S1), its redox speciation was obviously not controlled by the reaction
467 $0.25 \text{ O}_{2(\text{g})} + \text{H}^+ + \text{e}^- = 0.5 \text{ H}_2\text{O}$ (i.e. $\text{pH}+\text{pe} = 20.6$ for $p_{\text{O}_2} = 0.21 \text{ atm}$).

468 Calculations of Pu uptake on kaolinite are performed for the experimental conditions
469 of Banik et al. (2007). Constant redox conditions are considered. Only the results obtained for
470 $\text{pH} < 5$ will be discussed here. Regarding the uncertainty in the $\text{pH}+\text{pe}$ value, it is adjusted to
471 provide the best fit to the experimental data (Figure 4a). A relatively good fit is achieved for
472 $\text{pH}+\text{pe} = 16.2$, consistent with the estimate from the redox state analysis ($\text{pH}+\text{pe} \approx 16.1$).
473 Figure 4b shows a predominance diagram restricted to relevant pH-pe conditions for the study
474 of Banik et al. (2007). Only the aqueous redox speciation is shown because only Pu(IV) is
475 calculated to prevail at the kaolinite surface for $14 < \text{pH}+\text{pe} < 18$ (see Fig. 3a). Here, the
476 predominance diagram is plotted as $\text{pH}+\text{pe}$ versus pH (instead of pe versus pH) to visualize
477 constant redox conditions as a horizontal line. The comparison between the $\text{pH}+\text{pe} = 16.2$ line
478 and $\{\text{Pu}(\text{IV})/\text{Pu}(\text{III})\}_{\text{aq}}$ or $\{\text{Pu}(\text{V})/\text{Pu}(\text{IV})\}_{\text{aq}}$ can explain the features observed in the Pu uptake
479 curve. For $\text{pH} < 5$, Pu(III) and Pu(V) weakly sorb to kaolinite. Therefore, maximum uptake is
480 found when Pu(IV) dominates in solution, i.e. when physico-chemical conditions approach a
481 pure Pu(IV) system ($\text{pH} \approx 2$). The decreased uptake with increasing pH from 2 to 5 is due to
482 the predominance of Pu(V) in solution, which is very well predicted. Minimum uptake is
483 found when the difference between the line of the redox condition ($\text{pH}+\text{pe} = 16.2$) and the
484 line of $\{\text{Pu}(\text{V})/\text{Pu}(\text{IV})\}_{\text{aq}}$ reaches a maximum (shown as a double arrow in figure 4b; $4 < \text{pH}$
485 < 5). The present approach allows the description of overall Pu uptake on kaolinite, by
486 applying thermodynamic concepts and by simultaneously taking into account the complete Pu
487 redox chemistry and the respective sorption behavior. The calculations are very sensitive to pe,
488 as illustrated on figure 4 by considering $\text{pe} \pm 0.5$ (corresponding to $\pm 0.03 \text{ V}$). This result

489 clearly shows that without any information concerning the redox conditions in the experiment,
490 it is almost impossible to predict Pu uptake by kaolinite.

491 Above pH = 5, information about pe is not available. Simulations are made assuming
492 pH+pe = 16.2 as before. Because of the strong assumption, the following simulations and
493 discussion should be considered with caution. For pH = 9, Pu(IV) is the dominant redox state
494 in solution (see Fig. 4b), consistent with redox state analysis. For pH > 5, the solution is
495 oversaturated with respect to PuO_{2(am,hyd)}: total aqueous [Pu(IV)]_{tot,aq} equals approximately 10⁻⁹
496 M for pH = 9, whereas the Pu(IV) solubility limit is 10^{-10.4±0.5} M (Neck et al., 2007). The
497 break in the simulated curve (Fig. 4a) is due to the inclusion of Pu precipitation in the
498 calculations. Experimentally, precipitation (both homogeneous and heterogeneous) is difficult
499 to distinguish from the surface uptake processes. This leads to an overestimation of the overall
500 Pu uptake for pH > 5. Preliminary test calculations showed that this cannot be attributed to the
501 assumed redox conditions, as illustrated in Figure 4a when considering pe ± 0.5. Neck et al.
502 (2007) found that formation of Pu(IV) intrinsic (eigen-) colloids (PuO_{2(am,coll,hyd)}) leads to an
503 increased apparent solubility of Pu up to 10^{-8.3±1.0} M. Removal of these colloids from the
504 aqueous phase requires either ultrafiltration at 3-10 kDa or ultracentrifugation. Banik et al.
505 (2007) only performed phase separation by centrifugation at 3000g, which is not sufficient to
506 remove Pu(IV)-colloids. Furthermore, Banik et al. (2007) performed experiments for
507 approximately 10 and 50 times higher [Pu]_{tot} (6.6×10⁻⁸ M and 3.2×10⁻⁷ M). Experimentally
508 observed Pu uptake does not change but the corresponding calculations lead to an enhanced
509 uptake with increasing [Pu]_{tot} because of the increased amount of precipitated PuO_{2(am,hyd)} (see
510 Fig. S2). Although Pu(IV)-colloids interact with mineral surfaces (Reich et al. 2007; Powell et
511 al., 2011; Schmidt et al., 2012), a small fraction of Pu(IV)-colloids remained in the
512 supernatant in the experiments of Banik et al. (2007) because of insufficient phase separation.
513 It is also possible that, although thermodynamically favorable, PuO_{2(am,hyd)} was not formed

514 within 209 h in the presence of kaolinite. This is illustrated in Figure 4a (bold dashed line)
515 where we neglect the precipitation of $\text{PuO}_{2(\text{am,hyd})}$, which then leads to a better fit for $\text{pH} > 5$.
516 Indeed, as observed experimentally for $\text{pH} > 5$, an increasing Pu uptake with increasing pH is
517 predicted because the redox conditions approach the stability field of $\text{Pu(IV)}_{\text{aq}}$. Above $\text{pH} = 8$,
518 only Pu(IV) is found in solution for $\text{pH} + \text{pe} = 16.2$ and Pu uptake is predicted to be equal to
519 Th(IV). Unfortunately, the sorption of Pu-colloids to kaolinite cannot be simulated yet using
520 a mechanistic model without making additional assumptions. However, overall Pu uptake for
521 $\text{pH} = 8$ is similar to Th(IV), although significant amounts of Pu(IV)-colloids are present, and
522 is independent of $[\text{Pu}]_{\text{tot}}$ (Figure S2). Eq. 5 suggests that the respective K_d for aqueous Pu(IV)
523 and Pu(IV)-colloids are similar for $\text{pH} = 8$. This might be because $\text{Pu(OH)}_{4(\text{aq})}$ (i.e. the
524 prevailing aqueous Pu(IV) species) and $\text{PuO}_{2(\text{am,coll,hyd})}$ are both uncharged species at $\text{pH} = 8$
525 (Neck et al., 2007). However, the sorption of Pu(IV)-colloids to minerals needs to be studied
526 in further experiments.

527

528 3.3.2. Comparison with other systems

529 Various experimental studies were dedicated to Pu sorption on oxidic minerals. Under
530 oxidizing conditions (e.g. ambient air) Pu(V) was initially introduced (e.g. Powell et al., 2005;
531 Zavarin et al., 2012; Hixon et al., 2013: for goethite, hematite, montmorillonite and quartz,
532 respectively). These studies report a relatively fast and strong Pu uptake, which is due to the
533 presence of Pu(IV) on the surface whereas Pu(V) remained in solution. Equation 16 implies
534 that the thermodynamic stability field of the more strongly adsorbing Pu redox state is
535 enhanced at a mineral surface compared to the aqueous phase. The actinide pH-edge sequence
536 $\text{An(V)} < \text{An(III)} \approx \text{An(VI)} < \text{An(IV)}$ (Geckeis et al., 2013) is generally obtained for all
537 minerals with surface $-\text{OH}$ groups. Therefore, the Pu(V)/Pu(IV) boundary at a mineral
538 surface can be expected to be most strongly shifted to higher pe, especially in the low pH

539 region where An(V) sorption to minerals is weak. Furthermore, equation 16 exhibits a rather
540 generic form, since it is based on K_d values, and is not restricted to Pu, kaolinite or to a
541 specific surface complexation model. However, the present approach is based on
542 thermodynamic concepts and might only be applicable when equilibrium or steady states are
543 reached. For our treatment, the p_e is required, which is often not experimentally determined
544 for various reasons. Finally, sorption data for analogues are required, but not always available.
545 Therefore, the more general applicability of the present approach can only be tested on a
546 limited number of available studies.

547 Np sorption and redox speciation in the presence of illite was recently investigated
548 (Marsac et al., 2015). When added as Np(V) to an illite suspension under argon atmosphere,
549 higher Np uptake was measured compared to a previous study under ambient atmosphere
550 (Gorgeon, 1994). X-ray Absorption Spectroscopy and redox state analysis revealed a
551 significant amount of Np(IV) at the illite surface whereas Np(V) prevailed in solution. By
552 taking into account the experimental p_e and surface complexation of both Np(V) and Np(IV)
553 to illite edge sites, the results of these Np sorption experiment could be modeled. In that study,
554 the 2 Site Protolysis Non-Electrostatic Surface Complexation and Cation Exchange (2 SPNE
555 SC/CE; Bradbury and Baeyens, 2009) model was used. For instance, for $pH = 7$ and an ionic
556 strength of 0.1 M NaCl, $\log K_d(Np(V)) \approx 1.5$ L/kg and $\log K_d(Np(IV)) \approx 6$ L/kg. In agreement
557 with eq. 16, $\{Np(V)/Np(IV)\}_{surf}$ was found approximately 4.5 p_e units higher than
558 $\{Np(V)/Np(IV)\}_{aq}$ for these conditions. This simple calculation provides evidence that our
559 equations are applicable to another actinide, another mineral and another surface
560 complexation model.

561 Hixon et al. (2013) observed the reduction of Pu(V) to Pu(IV) at the quartz surface,
562 when working under ambient air conditions, and proposed that the strongly adsorbing Pu(IV)
563 is thermodynamically favored at the mineral surface compared to Pu(V), in agreement with

564 our approach. Hixon et al. (2013) more precisely calculated that, on quartz for pH = 7,
565 $\{Pu(V)/Pu(IV)\}_{surf}$ would need to be 0.28 V (4.7 pe units) higher than $\{Pu(V)/Pu(IV)\}_{aq}$ to
566 observe significant amounts of Pu(IV). Although a surface complexation model has been used
567 in the above cases to obtain a numerical equation describing $K_d(IV)$ and $K_d(V)$ versus pH, eq.
568 16 can directly be applied to empirical (measured) K_d values when available for the same
569 mineral and the same physico-chemical conditions. Since we did not find data for An(V) and
570 An(IV) sorption to quartz to quantitatively support the findings of Hixon et al. (2013),
571 sorption data for amorphous silica ($SiO_{2(am)}$) are used as an estimate. In addition, even though
572 K_d values for Th(IV) can directly be used for Pu(IV) sorption to kaolinite, this must be proven
573 to be true for other minerals because both elements show significantly different hydrolysis.
574 Consequently, the following estimates are based on strong assumptions and involve the
575 concomitant uncertainties. Equation 16, based on K_d , is empirical and it is recommended to
576 restrict its application to sorption data obtained for minerals of the same origin. This avoids for
577 instance handling variations in the surface area of the mineral used between separate studies.
578 To follow up on the quartz example, Righetto et al. (1991) studied both Th(IV) and Np(V)
579 sorption to amorphous silica ($SiO_{2(am)}$) in 0.1 M $NaClO_4$. Their data were recalculated to K_d
580 (L/kg) and are presented in figure S3. Th(IV) sorption data were recorded only up to pH = 3.5,
581 where a constant K_d is reached ($\log K_d = 4.7$ L/kg). Reiller et al. (2003) investigated Th(IV)
582 sorption to $SiO_{2(am)}$ and observed constant K_d up to pH = 9. Therefore, we can safely assume
583 constant K_d values for Th(IV) for pH > 3.5. Np(V) sorption is weak and $\log K_d(Np(V)) = 1.7$
584 L/kg for pH = 7. From this, we estimate $\{Pu(V)/Pu(IV)\}_{surf} - \{Pu(V)/Pu(IV)\}_{aq} = 3$, for pH =
585 7, i.e. the Pu(V)/Pu(IV) boundary at the $SiO_{2(am)}$ surface is approximately 0.18 V above the
586 one in solution. Despite the large uncertainties discussed above, our simple estimate is
587 qualitatively consistent with Hixon et al. (2013).

588 Interestingly, the shift in the p_e , $\{An(V)/An(IV)\}_{surf} - \{An(V)/An(IV)\}_{aq}$, is shown to
589 depend on the nature of the mineral, which equals +4.5 for illite, +2.5 for kaolinite (as can be
590 calculated from Np(V) and Th(IV) sorption to kaolinite data; figure 1) and +3 for $SiO_{2(am)}$.
591 We cannot provide a convincing explanation for this observation at present. Clearly this issue
592 will require a larger dataset for various minerals and more advanced calculations. In general,
593 all minerals discussed above consistently show the stabilization of Pu(IV) at their surface,
594 highlighting the importance of Pu(IV) even under slightly oxidizing conditions.

595 Because of its weak interaction with minerals, Pu(V) is known to be rather mobile.
596 The opposite is true for Pu(IV). Therefore, an accurate knowledge of the Pu(V)/Pu(IV) redox
597 couple is particularly important to predict Pu mobility in the environment. Although kinetic
598 aspects might be required in order to predict Pu mobility, the present study supports previous
599 experimental and modeling studies dedicated to the transport of Pu in (partially) oxygenated
600 soils or sediments (e.g. Kaplan et al., 2004; Powell et al., 2014) where Pu(V) was found to be
601 the mobile form of Pu (i.e. in the aqueous phase), whereas Pu(IV) was found at the surface of
602 the solids, being strongly bound and decreasing the amount of dissolved Pu(V) and
603 consequently limiting Pu transport. The strong interaction of Pu with minerals via the
604 stabilization of Pu(IV) at their surfaces over a wide range of pH-pe conditions also agrees
605 with the idea of colloid-facilitated transport of this element (Kersting et al., 1999; Xie et al.,
606 2013).

607

608 **3.4. Pu(IV) versus Pu(III)**

609 Buda et al. (2008) studied Pu(III) sorption to kaolinite, compared it to Am(III) data
610 and found the pH-edges to be very similar. The authors used $NH_2OH \cdot HCl$ as a reductant to
611 maintain the trivalent redox state of Pu. This was not efficient for $pH > 6$ and Pu(IV) was

612 formed in the absence of kaolinite. Therefore, above $\text{pH} = 6$, the redox potential falls within
613 the stability field of $\text{Pu(IV)}_{\text{aq}}$. Buda et al. (2008) could well describe Pu redox chemistry in the
614 presence of kaolinite, assuming the presence of Pu(IV) for $\text{pH} > 6$. The present study shows
615 that, different from other redox couples, $\{\text{Pu(IV)/Pu(III)}\}_{\text{surf}}$ is not significantly different from
616 $\{\text{Pu(IV)/Pu(III)}\}_{\text{aq}}$ for $\text{pH} > 6$ in 0.1 M NaClO_4 . For reducing conditions, the previous
617 discussions about Pu redox chemistry in contact with kaolinite based on the stability fields of
618 Pu(IV)/Pu(III) in solution might be correct, even if sorption processes are disregarded.

619 **3.5. Pu(VI) at the kaolinite surface?**

620 Our calculations suggest that Pu(VI) can be stable at the kaolinite surface for $\text{pH} + \text{pe} >$
621 18. This is not supported by any experimental results. To obtain Pu(IV) as the dominant redox
622 state at the kaolinite surface under $p_{\text{O}_2} = 0.21 \text{ atm}$, $\{\text{Pu(VI)/Pu(IV)}\}_{\text{surf}}$ must be at least ~ 2.5
623 log units higher than the presently calculated one, i.e. $\log K_{\text{d}}(\text{IV}) - \log K_{\text{d}}(\text{VI})$ must be about 5
624 (two electrons are involved). Obviously, this is beyond experimental uncertainties. As
625 discussed previously (see e.g. fig. 3b), even though prevailing at the surface, the overall
626 amount of Pu adsorbed to kaolinite can be low for a large range of pH under oxidizing
627 conditions. Furthermore, the present calculations are made in the absence of CO_2 whereas
628 experiments under oxidizing conditions are generally made under ambient atmosphere. U(VI)
629 sorption to kaolinite decreases from $\sim 95\%$ to $\sim 10\%$ between pH 8 and 9 in the presence of
630 carbonate (e.g. Payne et al., 2004; Křepelová 2007; Gao et al., 2010), which would, by
631 analogy, further limit Pu(VI) sorption to kaolinite although ternary kaolinite-Pu(VI)-carbonate
632 surface complexes might form. Such complexes have for instance been observed for U(VI) on
633 montmorillonite (Marques Fernandez et al., 2012). Consequently, the presence of Pu(VI) at
634 the kaolinite surface might be of limited relevance. Nevertheless, the fate of Pu(VI) at mineral
635 surfaces appears elusive at present. For instance, Romanchuk et al. (2011; 2013) observed
636 partial reduction to Pu(IV) in contact with hematite. Kumar et al. (2012) contacted Pu(IV)

637 with alumina and found some Pu(VI) in solution. Olsson et al. (2003) were able to stabilize
638 Pu(VI) in contact with TiO₂ and determined its pH-dependent sorption. Further work is
639 required to clarify the role of Pu(VI) under oxidizing conditions. Our survey of the available
640 data would suggest a dependence on the type of sorbing mineral.

641

642

643 **3.6. Further development required**

644 The present study focusses on experimental studies, where An sorption to kaolinite
645 was investigated in the absence of complexing ligands other than OH⁻, i.e. under conditions
646 different from the complexity of natural waters. For instance, carbonates and humic
647 substances are known to strongly affect An speciation and sorption to minerals. Reiller (2005)
648 evaluated the impact of both carbonates and humic acids (HA) on the redox speciation of
649 U/Np/Pu by applying thermodynamic calculations. Based on a similar approach (i.e.
650 speciation calculations at equilibrium), Reiller (2005) predicted a narrow predominance field
651 for Pu(V) due to strong Pu(VI)-carbonate and Pu(IV)-HA complexation, as in the present case,
652 where the predominance field arises from strong sorption of Pu(VI) and Pu(IV) at the
653 kaolinite surface. While metal ion complexation by various ligands can in principle be
654 included in the side reaction coefficient (eq. 12), no attempt is made here for the sake of
655 simplicity. The approach can be extended to account for the effect of other ligands in the
656 future. However, to predict Pu sorption and redox speciation at a mineral surface in the
657 presence of carbonates and HA, the formation of ternary surface complexes must be taken
658 into account. Such complexes were included in models for instance by Marques Fernandez et
659 al. (2008; 2012) for the Eu(III)- and U(VI)-monmorillonite-carbonate ternary systems. The
660 prediction of An sorption to minerals in the presence of humic substances is even more

661 complex and relies on an accurate description of the mechanisms controlling humic
662 substances sorption to minerals and the identification of the ternary complexes formed, which
663 is still under debate (see e.g. Reiller, 2012).

664

665

666

4. Conclusion

667 It is well known that Pu redox speciation has a strong impact on its mobility in the
668 environment. Various experimental studies have shown that mineral surfaces affect Pu redox
669 speciation. In the present study, Pu redox speciation at the kaolinite surface is interpreted
670 based on the thermodynamic stability of the respective Pu redox state at the surface. To
671 overcome difficulties in the interpretation of results related to the sensitivity of Pu to redox
672 conditions, uptake data on kaolinite of the more redox-stable Am(III), Th(IV), Np(V) and
673 U(VI) - chemical analogues for Pu(III,IV,V,VI) - are used to calibrate a surface complexation
674 model. To fully understand Pu redox chemistry in the aqueous kaolinite suspension, the
675 system is treated separately for the aqueous solution and the kaolinite surface, and the two
676 resulting Pu predominance diagrams are superimposed. This method visualizes how the
677 prevailing Pu redox states can differ between solution and surface for given pH/pe conditions.
678 Notably, the kaolinite surface has no impact on the Pu(IV)/Pu(III) distribution in neutral to
679 alkaline conditions, in the absence of aqueous ligands other than OH⁻. Therefore, the study of
680 Pu(III) sorption to minerals is relevant for the reducing conditions encountered in deep
681 geological nuclear waste repository sites. Under slightly oxidizing conditions, Pu(IV) can be
682 stabilized at the kaolinite surface within the stability field of Pu(V) in solution, which
683 significantly increases overall Pu uptake. The present model predicts overall experimental Pu
684 uptake when the Pu(V)/Pu(IV) redox couple is involved. This suggests that Pu-mineral
685 interaction is strong, even under slightly oxidizing condition. Also Pu(VI) can be stabilized at
686 the kaolinite surface within the stability field of Pu(V) in solution, under oxidizing conditions.
687 Its impact on overall Pu uptake is limited to redox conditions in equilibrium with ambient air
688 atmosphere (O₂), by the weak Pu(VI) sorption to kaolinite for pH < 5 and the strong Pu(VI)-
689 carbonate (due to atmospheric CO₂) complexation in alkaline conditions. Independent
690 experimental data for other minerals with Pu and with Np corroborate our approach. The

691 derived equations are of rather generic form making them easily applicable yet to other
692 adsorbant/adsorbat systems.

693 Based on the thermodynamic stability of the sorbed Pu species, the exact redox
694 mechanism does not need to be explicitly considered but the redox potential of the system
695 must be known. Measurement of redox potential is rarely simple and often bears large
696 uncertainties, but the pe (or Eh) strongly affects overall Pu uptake by kaolinite. A redox state
697 analysis of aqueous Pu can provide information on pe, when a steady state is reached. The
698 determination of pe from Pu redox state analysis heavily relies on the accuracy of the
699 available thermodynamic database for aqueous complexes, i.e. their capability to describe the
700 speciation of the different Pu redox states in presence of various ligands. This fact becomes
701 more important for natural samples that are more complex than the systems considered in this
702 work.

703

704 **Acknowledgements**

705 The authors gratefully thank Dr. David G. Kinniburgh for his advices and the development of
706 additional tools in Phreeplot after the authors request, Prof. Horst Geckeis, three anonymous
707 reviewers and Dr. Carla Koretsky (Associate Editor) for helpful comments. This work was
708 financed by the Federal Ministry of Economic Affairs and Energy (Germany) under contracts
709 No. 02E10206 and 02E10961.

710 **References**

- 711 Altmaier M., Gaona X. and Fanghänel Th. (2013) Recent Advances in Aqueous Actinide
712 Chemistry and Thermodynamics. *Chem. Rev.* **113**, 901-943.
- 713 Altmaier M., Gaona X., Fellhauer D. and Buckau G. (2010) Intercomparison of redox
714 determination methods on designed and near-neutral aqueous systems. KIT-SR 7572,
715 Karlsruhe Institute of Technology, Karlsruhe.
- 716 Amayri S., Jermolajev A. and Reich T. (2011) Neptunium(V) sorption on kaolinite,
717 *Radiochim. Acta* **99**, 349–357.
- 718 Banik (2006) Speciation of tetravalent plutonium in contact with humic substances and
719 kaolinite under environmental conditions. Ph.D. thesis, Johannes Gutenberg-University,
720 Mainz, Germany.
- 721 Banik N. L., Buda R. A., Bürger S., Kratz J. V. and Trautmann N. (2007) Sorption of
722 tetravalent plutonium and humic substances onto kaolinite. *Radiochim. Acta* **95**, 569-
723 575.
- 724 Bradbury M. H. and Baeyens B. (2005) Modelling the sorption of Mn(II), Co(II), Ni(II),
725 Zn(II), Cd(II), Eu(III), Am(III), Sn(IV), Th(IV), Np(V) and U(VI) on montmorillonite:
726 Linear free energy relationships and estimates of surface binding constants for some
727 selected heavy metals and actinides. *Geochim. Cosmochim. Acta* **69**(4), 875-892.
- 728 Bradbury M. H. and Baeyens B. (2006) Modelling sorption data for the actinides Am(III),
729 Np(V) and Pa(V) on montmorillonite. *Radiochim. Acta* **94**, 619–625.
- 730 Bradbury M. H. and Baeyens B. (2009) Sorption modeling on illite Part II: actinide sorption
731 and linear free energy relationships. *Geochim. Cosmochim. Acta.* **73**, 1004-1013.
- 732 Buda R. A., Banik N. L., Kratz J. V. and Trautmann N. (2008) Studies of the ternary systems
733 humic substances – kaolinite – Pu(III) and Pu(IV). *Radiochim. Acta* **96**, 657-665.
- 734 Choppin G. R. (1999) Utility of oxidation state analogs in the study of plutonium behavior.
735 *Radiochim. Acta* **85**, 89-95.
- 736 Ciavatta L. (1980) The specific interaction theory in evaluating ionic equilibria. *Annali di*
737 *Chimica* **70**, 551–567.
- 738 Dai M., Kelley J. M. and Buesseler K. O. (2002) Sources and migration of plutonium in
739 groundwater at the Savannah River Site. *Environ. Sci. Technol.* **36**, 3690-3699.
- 740 Davis J. A., Coston J. A., Kent D. B. and Fuller C. C. (1998) Application of the surface
741 complexation concept to complex mineral assemblages. *Environ. Sci. Technol.* **32**,
742 2820–2828.
- 743 Davis J. A., Meece D. E., Kohler M. and Curtis G. P. (2004) Approaches to surface
744 complexation modeling of Uranium (VI) adsorption on aquifer sediments. *Geochim.*
745 *Cosmochim. Acta* **68**, 3621–3641.
- 746 Gaines G. I. and Thomas H. C. (1953) Adsorption studies on clay minerals. II. A formulation
747 of the thermodynamics of exchange adsorption. *Journal of Physical Chemistry* **21**, 714-
748 718.

- 749 Gao L., Yang Z., Shi K., Wang X., Guo Z. and Wu W. (2010) U(VI) sorption on kaolinite:
750 effects of pH, U(VI) concentration and oxyanions. *J. Radioanal. Nucl. Chem.* **284**, 519-
751 526.
- 752 Geckeis H., Lützenkirchen J., Polly R., Rabung T. and Schmidt M. (2013) Mineral-Water
753 Interface Reactions of Actinides. *Chem. Rev.* **13**(2), 1016-1062.
- 754 Gorgeon L. (1994) Contribution à la modélisation physico-chimique de la rétention de
755 radioéléments à vie longue par des matériaux argileux. Ph.D. thesis, Université Paris 6.
- 756 Guillaumont R., Fanghänel Th., Fuger J., Grenthe I., Neck V., Palmer D. A. and Rand M. H.
757 (2003) Update on the Chemical Thermodynamics of Uranium, Neptunium, Plutonium,
758 Americium and Technetium, Mompean, F.J., Domenech-Orti, C., Ben-Said, K.,
759 OECD/NEA Data Bank, Eds., vol. 5 of Chemical Thermodynamics, Elsevier,
760 Amsterdam.
- 761 Hixon A. E. and Powell B. A (2014) Observed changes in the mechanism and rates of Pu(V)
762 reduction on hematite as a function of total plutonium concentration. *Environ. Sci.*
763 *Technol.* **48**, 9255-9262.
- 764 Hixon A. E., Arai Y. and Powell B. A. (2013) Examination of the effect of alpha radiolysis on
765 plutonium(V) sorption to quartz using multiple plutonium isotopes. *J. Coll. Int. Sci.* **403**,
766 105-112.
- 767 Kaplan D. I., Powell B. A., Demirkanli D. I., Fjeld R. A., Molz F. J., Serkiz S. M. and Coates
768 J. T. (2004) Influence of oxidation states on plutonium mobility during long-term
769 transport through an unsaturated subsurface environment. *Environ. Sci. Technol.* **38**,
770 5053-5058.
- 771 Kaplan D. I., Powell B. A., Duff M. C., Demirkanli D. I., Denham M., Fjeld R. A. and Molz F.
772 J. (2007) Influence of sources on plutonium mobility and oxidation state
773 transformations in vadose zone sediments. *Environ. Sci. Technol.* **41**, 7417-7423.
- 774 Kersting A. B. (2013) Plutonium Transport in the Environment. *Inorg. Chem.* **52**, 3533-3546.
- 775 Kersting A. B., Efurud D. W., Finnegan D. L., Rokop D. J., Smith D. K. and Thompson J. L.
776 (1999) Migration of plutonium in groundwater at the Nevada Test Site. *Nature* **397**, 56-
777 59.
- 778 Kinniburgh D. G. and Cooper D. M. (2009) PhreePlot: Creating graphical output with
779 PHREEQC. <<http://www.phreeplot.org>>.
- 780 Kirsch R., Fellhouer D., Altmaier M., Neck V., Rossberg A., Fanghänel Th., Charlet L. and
781 Scheinost A. C. (2011) Oxidation state and local structure of plutonium reacted with
782 magnetite, mackinawite, and chukanovite. *Environ. Sci. Technol.* **45**, 7267-7274
- 783 Křepelová A. (2007) Influence of humic acid on the sorption of uranium(VI) and
784 americium(III) onto kaolinite. Ph.D. thesis, Faculty of Mathematics and Natural Sciences,
785 University of Dresden, Germany.
- 786 Kumar S., Kasar S. U. and Tomar B. S. (2012) Interfacial sorption/desorption studies of
787 Pu(IV) on silica and alumina surfaces. *Radiochim. Acta* **100**, 885-892.
- 788 Lujanienė G., Šapolaitė J., Radžiutė E. and Aninkevičius V. (2009) Plutonium oxidation state
789 distribution in natural clay and goethite. *J. Radioanal. Nucl. Chem.* **282**, 793-797.

- 790 Lützenkirchen J. (2012) Summary of studies on (ad)sorption as a "well-established" process
791 within FUNMIG activities. *Appl. Geochem.* **27**, 427-443.
- 792 Lützenkirchen J., Abdelmonem A., Weerasooriya R., Heberling F., Metz V. and Marsac R.
793 (2014) Adsorption of dissolved aluminum on sapphire-c and kaolinite: implications for
794 points of zero charge of clay minerals. *Geochem. Trans.* **15**, 9.
- 795 Marques Fernandes M., Baeyens B. and Bradbury M. H. (2008) The influence of carbonate
796 complexation on lanthanide/actinide sorption on montmorillonite. *Radiochim. Acta* **96**,
797 691-697.
- 798 Marques Fernandes M., Baeyens B., Dähn R., Scheinost A. C. and Bradbury M. H. (2012)
799 U(VI) sorption on montmorillonite in the absence and presence of carbonate: A
800 macroscopic and microscopic study. *Geochim. Cosmochim. Acta* **93**, 262–277.
- 801 Marsac R., Banik N. L., Diascorn A., Kupcik T., Lützenkirchen J., Marquardt C. M., Schäfer
802 T., Schild D., Rothe J., Dardenne K. and Geckeis H. (2015) Neptunium redox speciation
803 at the illite surface. *Geochim. Cosmochim. Acta* **152**, 39-51.
- 804 Miller J. D., Nalaskowski J., Abdul B. and Du H. (2007) Surface characteristics of kaolinite
805 and other selected two layer silicate minerals. *Can. J. Chem. Eng.* **85**, 617-624.
- 806 Neck V., Altmaier M. and Fanghänel T. (2007) Solubility of plutonium hydroxides/hydrous
807 oxides under reducing conditions and in the presence of oxygen. *C. R. Chimie* **10**, 959-
808 977
- 809 Olsson M., Jakobsson A.-M. and Albinsson Y. (2003) Sorption of Pu(VI) onto TiO₂. *J. Coll.*
810 *Int. Sci.* **266**, 269-275.
- 811 Parkhurst D. L. and Appelo C. A. J. (1999) User's guide to PHREEQC (Version 2) – a
812 computer program for speciation, batch reaction, one-dimensional transport and inverse
813 geochemical calculation. Water-resources Investigation Report 99-4259, USGS, Denver,
814 Colorado, p. 312.
- 815 Payne T. E., Davis J. A., Lumpkin G. R., Chisari R. and Waite T. D. (2004) Surface
816 complexation model of uranyl sorption on Georgia kaolinite. *Appl. Clay Sci.* **26**, 151-
817 162.
- 818 Powell B. A., Dai Z., Zavarin M., Zhao P. and Kersting A. B. (2011) Stabilization of
819 plutonium nano-colloids by epitaxial distortion on mineral surfaces. *Environ. Sci.*
820 *Technol.* **45**, 2698–2703.
- 821 Powell B. A., Fjeld R. A., Kaplan D. I., Coates J. T. and Serkiz S. M. (2004) Pu(V)O₂⁺
822 adsorption and reduction by synthetic magnetite (Fe₃O₄). *Environ. Sci. Technol.* **38**,
823 6016-6024.
- 824 Powell B. A., Fjeld R. A., Kaplan D. I., Coates J. T. and Serkiz S. M. (2005) Pu(V)O₂⁺
825 adsorption and reduction by synthetic hematite and goethite. *Environ. Sci. Technol.* **39**,
826 2107-2114.
- 827 Powell B. A., Kaplan D. I., Serkiz S. M., Coates J. T. and Fjeld R. A. (2014) Pu(V) transport
828 through Savannah River Site soils - an evaluation of a conceptual model of surface-
829 mediated reduction to Pu (IV). *J. Environ. Radioactiv.* **131**, 47-56.

- 830 Reich T., Reich T. Y., Amayri S., Drebert J., Banik N. L., Buda R. A., Kratz J. V. and
831 Trautmann N. (2007) Application of XAFS spectroscopy to actinide environmental
832 science. *AIP Conf. Proc.* **882**, 179-183.
- 833 Reiller P. (2005) Prognosticating the humic complexation for redox sensitive actinides
834 through analogy, using the charge neutralisation model. *Radiochim. Acta* **93**, 43-55.
- 835 Reiller P. (2012) Modelling metal–humic substances–surface systems: reasons for success,
836 failure and possible routes for peace of mind. *Min. Mag.* **76**, 2643–2658.
- 837 Reiller P., Moulin V., Casanova F. and Dautel C. (2003) On the study of Th(IV)-humic acid
838 interactions by competition sorption studies with silica and determination of global
839 interaction constants. *Radiochim. Acta* **91**, 513-524.
- 840 Righetto L., Bidoglio G., Azimonti G. and Bellobono I. R. (1991) Competitive actinide
841 interactions in colloidal humic acid-mineral oxide systems. *Environ. Sci. Technol.*
842 **25**(11), 1913-1919.
- 843 Romanchuk A. Y., Kalmykov S. N. and Aliev R. A. (2011) Plutonium sorption onto hematite
844 colloids at femto- and nanomolar concentrations. *Radiochim. Acta* **99**, 137-144.
- 845 Romanchuk A. Y., Kalmykov S. N., Egorov A. V., Zubavichus Y. V., Shiryaev A. A., Batuk
846 O. N., Conradson S. D., Pankratov D.A. and Presnyakov I. A. (2013) Formation of
847 crystalline $\text{PuO}_{2+x} \cdot n\text{H}_2\text{O}$ nanoparticles upon sorption of Pu(V,VI) onto hematite.
848 *Geochim. Cosmochim. Acta* **121**, 29-40.
- 849 Schmidt M., Wilson R. E., Lee S. S., Soderholm L. and Fenter P. (2012) Adsorption of
850 plutonium oxide nanoparticles. *Langmuir* **28**, 2620-2627.
- 851 Schüring J., Schulz H. D., Fischer W. R., Böttcher J. and Duijnsveld W. H. M. (2000) Redox:
852 fundamentals, processes and applications. Springer-Verlag Berlin Heidelberg New York.
853 251 p.
- 854 Tertre E., Castet S., Berger G., Loubet M. and Giffaut E. (2006) Surface chemistry of
855 kaolinite and Na-montmorillonite in aqueous electrolyte solutions at 25 and 60°C:
856 Experimental and modeling study. *Geochim. Cosmochim. Acta* **70**, 4579-4599.
- 857 Tertre E., Hofmann A. and Berger G. (2008) Rare earth element sorption by basaltic rock:
858 Experimental data and modeling results using the "Generalised Composite approach".
859 *Geochim. Cosmochim. Acta* **72**, 1043–1056.
- 860 Walther C. and Denecke M. A. (2013) Actinide colloids and particles of environmental
861 concern. *Chem. Rev.* **113**(2), 995-1015.
- 862 Xie J., Lu J., Lin J., Zhou X., Li M., Zhou G. and Zhang J. (2013) The dynamic role of natural
863 colloids in enhancing plutonium transport through porous media. *Chem. Geol.* **360-361**,
864 134-141.
- 865 Yun J.-I., Cho H.-R., Neck V., Altmaier M., Seibert A., Marquardt C. M., Walther C. and
866 Fanghänel Th. (2007) Investigation of the hydrolysis of plutonium(IV) by a
867 combination of spectroscopy and redox potential measurements. *Radiochim. Acta* **95**,
868 89-95.

869 Zaravin M., Powell B. A., Bourbin M., Pihong Zhao P. and Kersting A. B. (2012) NpO_2^+
870 and Pu(V) ion exchange and surface-mediated reduction mechanisms on
871 montmorillonite, *Environ. Sci. Technol.* **46**, 2692-2698.

872

873 **Table and figure caption**

874 **Table 1.** Thermodynamic constants at zero ionic strength used in the present study
875 (Guillaumont et al., 2003). The missing hydrolysis constants for Pu are taken from the
876 corresponding analogues (in brackets). Surface complexation constants for Pu(III, IV, V, VI)
877 are obtained assuming that the experimental uptake data of Am(III), Th(IV), Np(V) and U(VI)
878 by kaolinite are representative for the uptake of the corresponding Pu redox states. (*)
879 Exchange and surface complexation constants have been determined by Tertre et al. (2008).
880 Some constants could not be determined since no appropriate experimental data were
881 available. According to Tertre et al. (2006, 2008), the surface area of kaolinite is 10 m²/g, site
882 density for ≡SOH and exchange sites are 1.66 and 3.70 μmol/m², respectively.

883 **Figure 1.** Experimental sorption data (K_d , in L/kg) on kaolinite versus pH for actinides with
884 different redox states (Am(III)/Th(IV)/Np(V); data from Buda et al. (2008), Banik et al. (2007)
885 and Amayri et al. (2011), respectively) for 0.1 M NaClO₄. Data for U(VI) are taken from
886 Křepelová (2007) for 0.1 M NaClO₄ in the presence of CO₂ (closed diamonds; pH < 8) and
887 0.01 M NaClO₄ in the absence of CO₂ (open diamonds). The elements are considered as
888 chemical analogues for Pu(III/IV/V/VI). Pu(IV) data are recalculated from the sorption data
889 and Pu redox state analysis of Banik (2006) using eq. 17 (two large white circles). Curves
890 represent the modeled result for each Pu redox state.

891 **Figure 2.** Linear free energy relationship (LFER) between surface complexation $^S K_{X,(i-1)}$ and
892 hydrolysis constants $^{OH} K_{X,i}$. “X” is Pu redox state and “i” is the number of OH⁻ involved in
893 the complex, within the present model for kaolinite obtained by fitting Pu(III), Pu(IV), Pu(V)
894 and Pu(VI) surface complexation constant to the experimental Am(III), Th(IV), Np(V) and
895 U(VI) sorption to kaolinite data from the literature. All in 0.1 M NaClO₄.

896 **Figure 3.** (a) Overlay of Pu predominance plots in solution (thin black lines) and at the
897 kaolinite surface (bold gray lines). Only the predominance field of each redox state is shown,
898 not the detailed speciation (e.g. hydrolyzed species). (b) More common predominance
899 diagram where only the dominant Pu redox state can be seen for the total system (S/V = 4 g/L;
900 [NaClO₄] = 0.1 M; [Pu]_{tot} = 10⁻¹¹ M).

901 **Figure 4.** (a) Percentage uptake of Pu and Th by kaolinite ([Pu]_{tot} = 6.6 × 10⁻⁹ M / [Th]_{tot} = 6.6
902 × 10⁻¹³ M; 0.1 M NaClO₄; S/V = 4 g/L; either under ambient air below pH = 8 or argon
903 atmosphere) experimentally obtained by Banik et al. (2007) and calculated for pH+pe = 16.2,

904 considering (bold line) or not (bold dashed line) the precipitated $\text{PuO}_{2(\text{am})}$ to be removed from
905 the aqueous phase with the kaolinite. The model sensitivity to pe is illustrated applying ± 0.5
906 uncertainty on the pe: $\text{pH} + \text{pe} = 15.7$ (dashed line) and 16.7 (dashed-dotted line); precipitated
907 $\text{PuO}_{2(\text{am})}$ is considered to have been removed with kaolinite. (b) Predominance diagram for the
908 aqueous solution plotting $\text{pH} + \text{pe}$ versus pe to visualize constant redox conditions horizontally.
909 The legend is valid for (a) and (b).

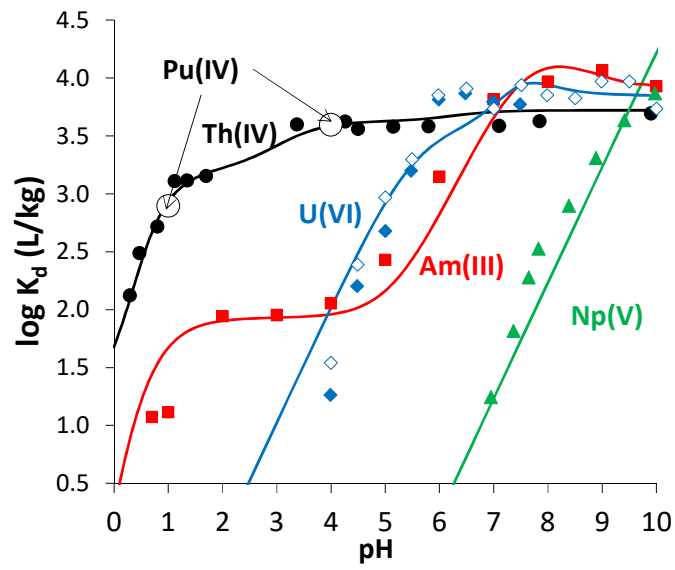
910

	Reaction	Log K (I = 0)
Solubility	$\text{PuO}_{2(\text{am,hyd})} + 2 \text{H}_2\text{O} = \text{Pu}^{4+} + 4 \text{OH}^-$	-58.33
Redox	$\text{PuO}_2^{2+} + \text{e}^- = \text{PuO}_2^+$	15.82
	$\text{PuO}_2^{2+} + 4 \text{H}^+ + 2 \text{e}^- = \text{Pu}^{4+} + 2 \text{H}_2\text{O}$	33.27
	$\text{PuO}_2^+ + 4 \text{H}^+ + \text{e}^- = \text{Pu}^{4+} + 2 \text{H}_2\text{O}$	17.45
	$\text{Pu}^{4+} + \text{e}^- = \text{Pu}^{3+}$	17.69
Hydrolysis	$\text{PuO}_2^{2+} + \text{H}_2\text{O} = \text{PuO}_2\text{OH}^+ + \text{H}^+$	-5.50
	$\text{PuO}_2^{2+} + 2 \text{H}_2\text{O} = \text{PuO}_2(\text{OH})_2 + 2 \text{H}^+$	-13.20
	$\text{PuO}_2^{2+} + 3 \text{H}_2\text{O} = \text{PuO}_2(\text{OH})_3^- + 3 \text{H}^+$	-20.25 (U)
	$\text{PuO}_2^{2+} + 4 \text{H}_2\text{O} = \text{PuO}_2(\text{OH})_4^{2-} + 4 \text{H}^+$	-32.40 (U)
	$\text{PuO}_2^+ + \text{H}_2\text{O} = \text{PuO}_2\text{OH} + \text{H}^+$	-11.30 (Np)
	$\text{PuO}_2^+ + 2 \text{H}_2\text{O} = \text{PuO}_2(\text{OH})_2^- + 2 \text{H}^+$	-23.60 (Np)
	$\text{Pu}^{4+} + \text{H}_2\text{O} = \text{PuOH}^{3+} + \text{H}^+$	0.60
	$\text{Pu}^{4+} + 2 \text{H}_2\text{O} = \text{Pu}(\text{OH})_2^{2+} + 2 \text{H}^+$	0.60
	$\text{Pu}^{4+} + 3 \text{H}_2\text{O} = \text{Pu}(\text{OH})_3^+ + 3 \text{H}^+$	-2.30
	$\text{Pu}^{4+} + 4 \text{H}_2\text{O} = \text{Pu}(\text{OH})_4 + 4 \text{H}^+$	-8.50
	$\text{Pu}^{3+} + \text{H}_2\text{O} = \text{PuOH}^{2+} + \text{H}^+$	-6.90
	$\text{Pu}^{3+} + 2 \text{H}_2\text{O} = \text{Pu}(\text{OH})_2^+ + 2 \text{H}^+$	-15.10 (Am)
	$\text{Pu}^{3+} + 3 \text{H}_2\text{O} = \text{Pu}(\text{OH})_3 + 3 \text{H}^+$	-26.20 (Am)
Exchange	$2 \text{X-Na} + \text{PuO}_2^{2+} = \text{X}_2\text{-PuO}_2 + \text{Na}^+$	nd
	$\text{X-Na} + \text{PuO}_2^+ = \text{X-PuO}_2 + \text{Na}^+$	nd
	$3 \text{X-Na} + \text{Pu}^{3+} = \text{X}_3\text{-Pu} + \text{Na}^+$	1
	$4 \text{X-Na} + \text{Pu}^{4+} = \text{X}_4\text{-Pu} + \text{Na}^+$	nd
	$\text{X-Na} + \text{H}^+ = \text{X-H} + \text{Na}^+$	-1 ^(*)
Surface complexation	$\equiv\text{SOH} + \text{PuO}_2^{2+} = \equiv\text{SO-PuO}_2^+ + \text{H}^+$	0.2
	$\equiv\text{SOH} + \text{PuO}_2^{2+} + \text{H}_2\text{O} = \equiv\text{SO-PuO}_2\text{OH} + \text{H}^+$	-6.9
	$\equiv\text{SOH} + \text{PuO}_2^{2+} + 2 \text{H}_2\text{O} = \equiv\text{SO-PuO}_2(\text{OH})_2^- + 3 \text{H}^+$	-14.5
	$\equiv\text{SOH} + \text{PuO}_2^+ = \equiv\text{SO-PuO}_2 + \text{H}^+$	-4.0
	$\equiv\text{SOH} + \text{Pu}^{4+} = \equiv\text{SO-Pu}^{3+} + \text{H}^+$	nd
	$\equiv\text{SOH} + \text{Pu}^{4+} + \text{H}_2\text{O} = \equiv\text{SO-PuOH}^{2+} + 2 \text{H}^+$	6.0
	$\equiv\text{SOH} + \text{Pu}^{4+} + 2 \text{H}_2\text{O} = \equiv\text{SO-Pu}(\text{OH})_2^+ + 3 \text{H}^+$	3.2
	$\equiv\text{SOH} + \text{Pu}^{4+} + 3 \text{H}_2\text{O} = \equiv\text{SO-Pu}(\text{OH})_3 + 4 \text{H}^+$	-3.0
	$\equiv\text{SOH} + \text{Pu}^{3+} = \equiv\text{SO-Pu}^{2+} + \text{H}^+$	-0.5 ^(*) (Eu)
	$\equiv\text{SOH} + \text{Pu}^{3+} + \text{H}_2\text{O} = \equiv\text{SO-PuOH}^+ + 2 \text{H}^+$	-9.3

911

912

Table 1



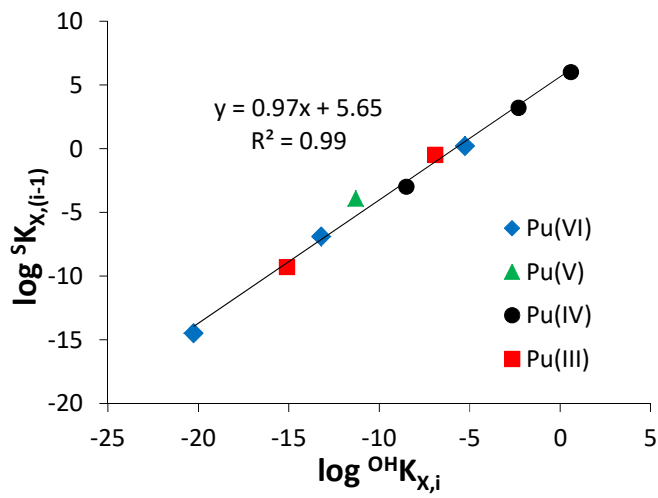
913

914

Figure 1

915

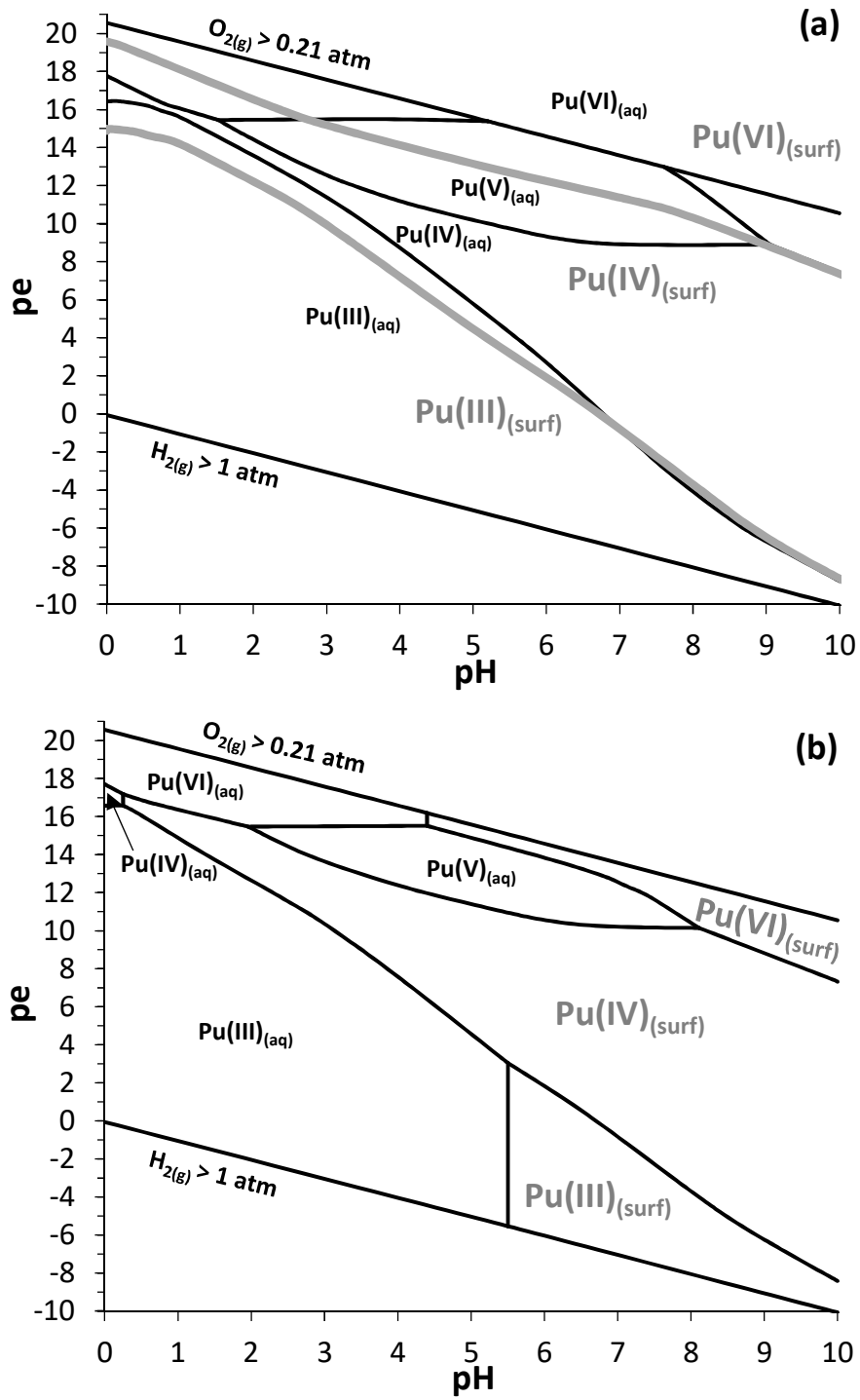
916



917

918

Figure 2

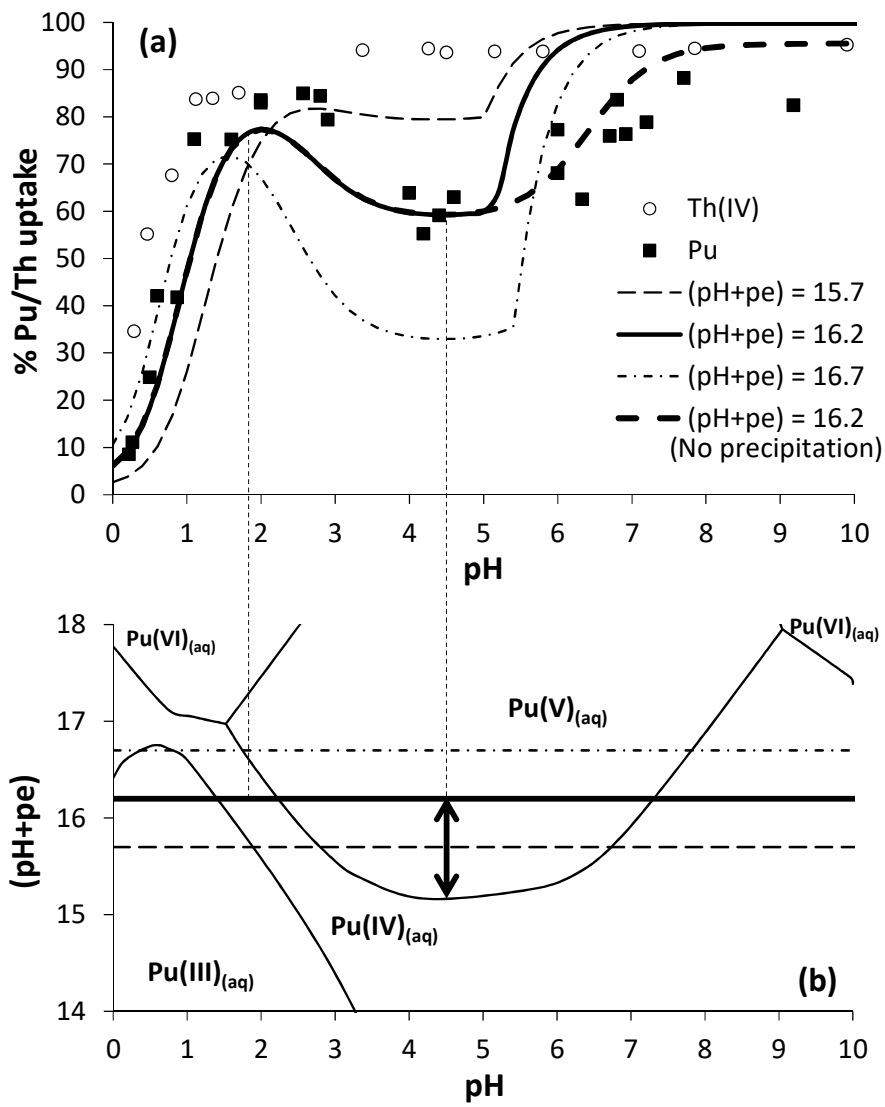


919

920

921

Figure 3



922

923

924

Figure 4

925 **Supporting information.**

926

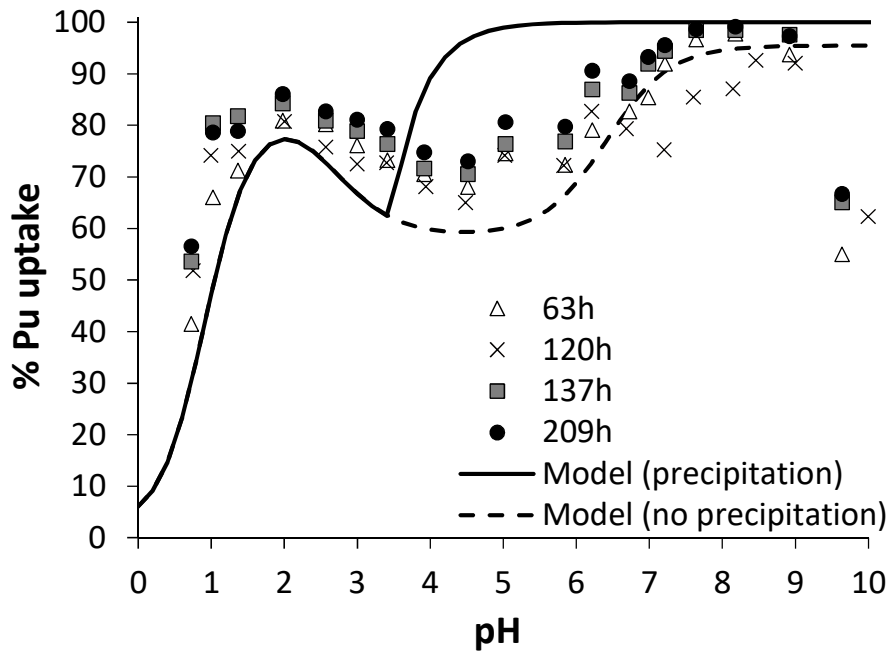
927 **Figure S1.** Percentage of Pu uptake in presence of kaolinite versus the pH for different
928 equilibration time (63, 120, 137, 209 hours). The results for $t = 120$ h were obtained for an
929 independent set of experiments. Experimental conditions: $S/V = 4$ g/L; $[Pu]_{tot} = 3.5 \times 10^{-7}$ M ;
930 0.1 M $NaClO_4$; ambient air atmosphere. Curves are simulations with the present model when
931 considering or not the precipitation of $PuO_{2(am)}$ as an uptake process ($pH+pe = 16.2$). The
932 effect of carbonate is not considered in the calculations.

933 **Figure S2.** Percentage of Pu uptake in presence of kaolinite versus the pH for different total
934 Pu concentrations ($[Pu]_{tot} = 6.9 \times 10^{-9}$; 6.6×10^{-8} ; 3.5×10^{-7} M). Experimental conditions: $S/V =$
935 4 g/L; 0.1 M $NaClO_4$; 120 h equilibration time; ambient air atmosphere. Curves are
936 simulations with the present model when considering or not the precipitation of $PuO_{2(am)}$ as an
937 uptake process ($pH+pe = 16.2$). The arrow shows the effect of increasing $[Pu]_{tot}$ on the
938 simulations. When no precipitation is considered, the same simulated results are obtained for
939 all $[Pu]_{tot}$. The effect of carbonate is not considered in the calculations.

940 **Figure S3.** Th(IV) and Np(V) sorption to amorphous silica versus the pH in 0.1 M $NaClO_4$
941 taken from Righetto et al. (1991) and recalculated as $\log K_d$ (L/kg). Experimental conditions:
942 $[Th]_{tot} = 10^{-11}$ M; $S/V = 60$ mg/L / $[Np(V)]_{tot} = 10^{-14}$ M; $S/V = 1200$ mg/L. The double arrow
943 illustrates $\log K_d(Th(IV)) - \log K_d(Np(V))$ for $pH = 7$ (see the main article).

944

945



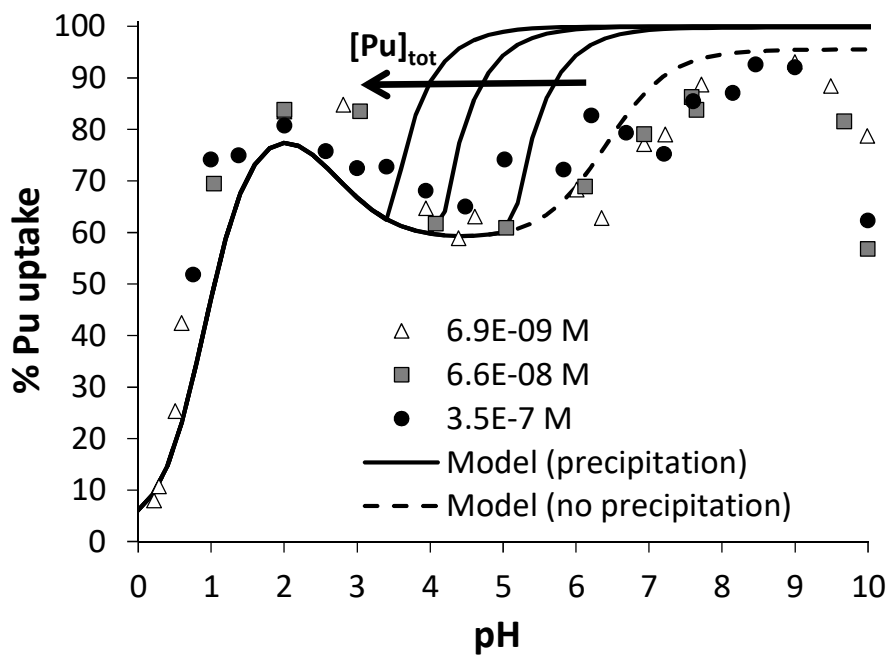
946

947

Figure S1

948

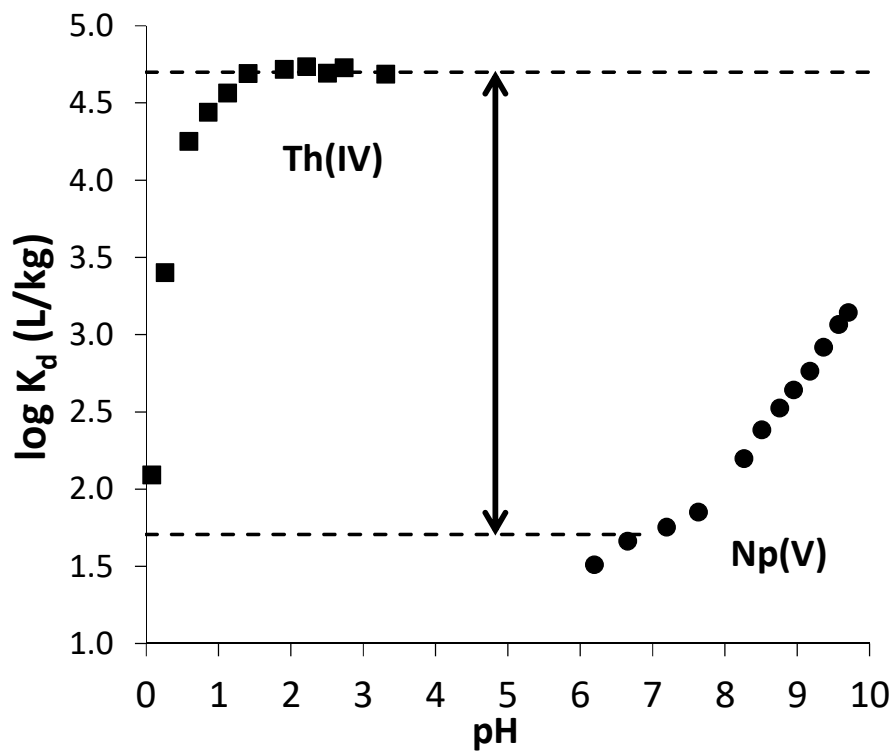
949



950

951

Figure S2



952

953

954

Figure S3